AEDC-TR-68-111

# STUDIES OF ELECTRICAL CHARACTERISTICS OF GASDYNAMIC BOUNDARY LAYERS IN SEEDED DIATOMIC GASES

E. E. Goins, Captain, USAF
Wendell Norman, ARO, Inc.

June 1968



*VON KÁRMÁN GAS DYNAMICS FACILITY*
*ARNOLD ENGINEERING DEVELOPMENT CENTER*
*AIR FORCE SYSTEMS COMMAND*
*ARNOLD AIR FORCE STATION, TENNESSEE*

# NOTICES

When U. S. Government drawings specifications, or other data are used for any purpose other than a definitely related Government procurement operation, the Government thereby incurs no responsibility nor any obligation whatsoever, and the fact that the Government may have formulated, furnished, or in any way supplied the said drawings, specifications, or other data, is not to be regarded by implication or otherwise, or in any manner licensing the holder or any other person or corporation, or conveying any rights or permission to manufacture, use, or sell any patented invention that may in any way be related thereto.

Qualified users may obtain copies of this report from the Defense Documentation Center.

References to named commercial products in this report are not to be considered in any sense as an endorsement of the product by the United States Air Force or the Government.

# STUDIES OF ELECTRICAL CHARACTERISTICS OF GASDYNAMIC BOUNDARY LAYERS IN SEEDED DIATOMIC GASES

E. E. Goins, Captain, USAF
Wendell Norman, ARO, Inc.



AF—AEDC
Arnold AFS Tenn

## FOREWORD

The work reported herein was sponsored by Headquarters, Arnold Engineering Development Center (AEDC), Air Force Systems Command (AFSC), under Program Element 6241003F, Project 7778, Task 777807.

The results of research presented were obtained by ARO, Inc. (a subsidiary of Sverdrup & Parcel and Associates, Inc.), contract operator of AEDC, AFSC, Arnold Air Force Station, Tennessee, under Contract AF40(600)-1200. The research was conducted at various times within the period July 1966 to January 1968 under ARO Project Nos. VJ3708 and VJ3821, and the manuscript was submitted for publication on April 24, 1968.

The authors wish to acknowledge the contributions of Jack Rose, VKF, who was in charge of the operation of the shock tube, and Dave Bynum and Richard Hudgens, VKF-Instrumentation, who developed the instrumentation used in the tests.

This technical report has been reviewed and is approved.

Charles V. Bennett
Acting Chief
Technical Facility
Development Division
Directorate of Plans
and Technology

Edward R. Feicht
Colonel, USAF
Director of Plans
and Technology

## ABSTRACT

Calculations are presented of the excess boundary-layer voltage drop attributable to the conduction of current through a thermal boundary layer on the electrodes of an MHD accelerator operating with seeded air or nitrogen, using the two-temperature model of Kerrebrock. For a laminar boundary layer, the excess boundary-layer voltage drop is found to be a linear function of pressure, relatively insensitive to free-stream temperature and seed fraction, and larger for air than for nitrogen. Experiments conducted in a shock tube showed an asymmetry in the voltage distribution for seeded air, with the cathode drop approximately 30 v and the anode drop approximately 10 v.

## CONTENTS



## ILLUSTRATIONS

## APPENDIX



## NOMENCLATURE

| | |
|---|---|
| $A_e$ | Area of effective electrodes |
| C | Capacitance of each can in transmission line |
| $C_A$ | Defined by Eq. (10) |
| D | Diameter of tube |
| E | Electric field strength |
| e | Electronic charge = $1.60207 \times 10^{-19}$ coulombs |
| h | Static enthalpy |
| h | Planck's constant = $6.625 \times 10^{-34}$ joule-sec |
| I | Total current |
| $I_p$ | Ionization potential |
| J | Current density |
| K | Equilibrium constant |
| k | Boltzmann's constant = $1.3804 \times 10^{-23}$ joule/°K |
| L | Inductance of each inductor in transmission line |
| M | Molecular weight |
| $M_s$ | Shock Mach number |
| m | Mass of particle |
| n | Number density |
| P | Pressure |
| $Q_e$ | Collision cross-section for electrons |
| R | Resistance |
| S | Seed fraction, by weight (Eq. (9)) |

| | |
|---|---|
| $T$ | Temperature |
| $t$ | Time |
| $t_d$ | Discharge time of transmission line |
| $t_r$ | Rise time for transmission line |
| $U$ | Flow velocity |
| $V_G$ | Voltage difference across electrodes during run |
| $V_1$ | Excess boundary-layer voltage drop at 1 atm |
| $V_i$ | Initial voltage across electrodes |
| $\Delta V$ | Voltage difference |
| $\Delta V_A$ | Voltage drop at anode |
| $\Delta V_C$ | Voltage drop at cathode |
| $\Delta V_{sheath}$ | Voltage drop at sheath |
| $X$ | Defined by Eq. (14) |
| $Y_{ch}$ | Effective height of equivalent rectangular channel |
| $Y_{eff}$ | Effective pin location in equivalent rectangular channel |
| $Y$ | Distance from electrode |
| $Z_o$ | Characteristic impedance of transmission line |
| $\delta$ | Electron collision energy loss parameter |
| $\delta$ | Boundary-layer thickness |
| $\epsilon_o$ | Permittivity of free space $\approx 10^{-9}/36\pi$ farad/m |
| $\sigma$ | Scalar conductivity |
| $\tau_{e,k}$ | Mean time between collisions of electron with particle species k |
| $\phi$ | Degree of ionization |

**SUBSCRIPTS**

| | |
|---|---|
| A | Base gas |
| BL | Boundary layer |
| e | Electron |
| i | Ion |

| | |
|---|---|
| k | Species k |
| n | Neutral |
| ns | Seed neutral |
| s | Seed |
| w | Wall |

**For Shock Tube**

| | |
|---|---|
| 1 | Conditions in front of incident shock |
| 2 | Conditions behind incident shock |
| 4 | Driver conditions |

**For Voltage Distributions (Table II and Fig. 18)**

| | |
|---|---|
| 1-5 | Pin numbers |
| $\infty$ | Outer edge of boundary layer |

# SECTION I
# INTRODUCTION

The voltage drop that results from reduced conductivity in the boundary layer of a cold electrode MHD accelerator must be accounted for in power supply selection. The boundary-layer voltage drop for such a device may be compensated for by increasing the voltage of the power supply. However, it is important that reasonable estimates of the magnitude of the boundary-layer voltage drops be available since:

a. Accelerators are usually made as small as possible in order to limit magnetic field energy requirements, and therefore, boundary layers represent a large percentage of the accelerator diameter.

b. The reduced electrical conductivity in high density boundary layers could result in voltage drops that could determine the major portion of electric field requirements.

Theoretical descriptions of the boundary-layer electrical phenomena for flows over cold electrodes have been offered (Refs. 1 and 2) and are presently being pursued (Ref. 3). The complexity of these analyses, their limitation to a narrow range of parameters, and lack of experimental verification make them somewhat impractical for use in design. Electrical characteristics of plasmas flowing adjacent to cold electrodes have been experimentally investigated and reported on by several authors (Refs. 4-9). Results of these investigations show that the plasma is composed of at least three regions, as shown in the simplified schematic presented as Fig. 1. Current is flowing into the cathode. Adjacent to the electrode is a sheath region within which charge neutrality is not preserved. This region is usually quite thin, of the order of a Debye length (Refs. 3, 7, and 10). It is found that at normal pressure (1 atm or less), the greatest portion of the voltage drop occurs within this region. A theoretical model of the sheath region that yields quantitative values of the drops for a wide range of conditions is not available.

This report is concerned with the region above the sheath, but within the gas dynamic boundary layer, for which charge neutrality is preserved. Because of the thermal boundary layer resulting from the relatively cold wall, the electrical conductivity based upon the gas temperature is quite low. However, conservation of current requires that a mechanism be provided in this region of reduced conductivity that will permit closing the circuit between the electrode and the diffuse discharge occurring in the free-stream flow. The mechanism assumed here is that

within the boundary-layer region, Joulean heating of the electrons causes them to achieve a temperature above that of the bulk gas, with a corresponding increase in electrical conductivity. An alternate model is that the current transverses the cold region in arcs. Although this latter model is almost certainly valid for the sheath region, it is not obvious which model is appropriate for the outer boundary layer.

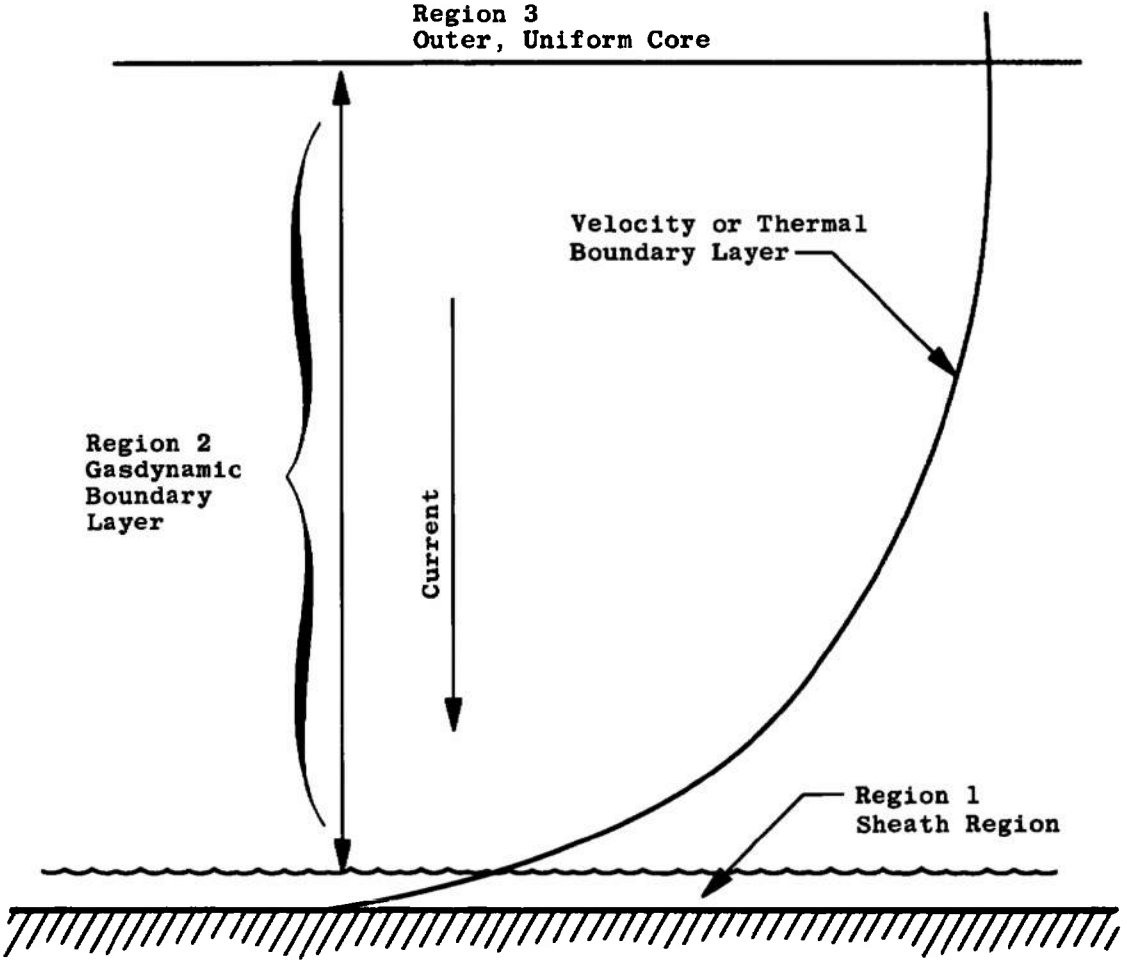


Fig. 1 Simplified Schematic of Flow over a Cold Cathode

The assumed current conduction model for this investigation is a very simple one in comparison with more involved analyses that are currently being performed. Argyropoulos et al. (Ref. 3) are currently investigating the problem including the effects of:

a. Elevated electron temperature

b. Electron radiation heat loss

c. Ion-slip effects

d. Flow velocity

e. Thermal gradients

f. Two-dimensional (Hall) effects (in the manner of Ref. 11 and many others)

g. Nonequilibrium thermal properties of the gas

The approach here is much simplified by comparison since only the first item in the above list is considered in the conductivity calculations.

The results of the experiments reported herein do not provide sufficient information to completely explain the mechanisms that provide current transmission through the boundary-layer region. However, the results generally support the validity of the assumed theoretical model for use in engineering estimates for voltage drops adjacent to cold electrodes.

## SECTION II
## CALCULATIONS OF CONDUCTIVITY AND VOLTAGE DROP

### 2.1 CONDUCTIVITY MODEL

The model used here to calculate the conductivity is the two-temperature model proposed by Kerrebrock (Ref. 12) in 1962 and since then extensively used. It is assumed that the fluid is composed of two gases, one consisting of the electrons, the other of the heavy particles. The electron gas is assumed to have a Maxwellian velocity distribution at a temperature which may be higher than that of the heavy gas. The temperature of the electron gas is found by a steady-state energy balance, accounting for the energy transferred to the electron gas from the electric field, and the energy transferred from the electron gas by collisions to the heavy particles. There are other modes of energy transfer, such as radiation and convection, which for the conditions of interest here may be neglected. The electron energy equation may then be written in the following form:

$$\frac{J^2}{\sigma} = \frac{3}{2} k n_e \sum_k \delta_k \frac{m_e}{m_k} \tau_{e,k}^{-1} (T_e - T_A) \qquad (1)$$

In this equation

J = current density, amp/m$^2$

$\sigma$ = scalar conductivity, mho/m

$k$ = Boltzmann's constant = $1.3804 \times 10^{-23}$ joule/°K

$n_e$ = electron number density, particles/$m^3$

$\delta_k$ = collision energy loss parameter for collisions between electrons and particles of species k

$m_e$ = mass of electron = $9.108 \times 10^{-31}$ Kg

$m_k$ = mass of particle of species k

$T_e$ = temperature of electron gas

$T_A$ = temperature of gas composed of heavy particles (assumed the same for all heavy species)

$\tau_{e,k}$ = mean time between collisions of electron and particles of species k

An expression for $\tau_{e,k}$ is (Ref. 3)

$$\tau_{e,k}^{-1} = \frac{4}{3} n_k \left(\frac{8k T_e}{\pi m_e}\right)^{1/2} Q_{ek} \tag{2}$$

in which

$n_k$ = number of species k, particles/$m^3$

$Q_{ek}$ = cross-section for collisions between electrons and particles of species k, $m^2$

The left-hand side of Eq. (1) is an expression for the Joulean heating of the electron gas. The right-hand side is the rate of energy transfer from the electron gas to the particles of the k species. Combining Eqs. (1) and (2) gives

$$\frac{J^2}{\sigma} = 4k (T_e - T_A) n_e \sqrt{\frac{2k T_e m_e}{\pi}} \sum_k \frac{\delta_k n_k Q_{ek}}{m_k} \tag{3}$$

The conductivity is expressed in the form presented in Ref. 14.

$$\sigma = \frac{0.532 n_e e^2}{\sqrt{m_e k T_e}} \left[\sum_k n_k Q_{ek}\right]^{-1} \tag{4}$$

in which

$e$ = electronic charge = $1.60207 \times 10^{-19}$ coulombs

### 2.1.1 Number Densities

In the two-temperature conductivity model, the number density of electrons, $n_e$, is assumed to be the same as the equilibrium value based on the electron temperature, $T_e$. Using this assumption and other relations, the number densities appearing in Eqs. (3) and (4) can be determined.

It is assumed that all of the electrons come from the ionization of the seed material. The ionization reaction is

$$K + M \rightleftarrows K^- + e - M$$

in which M is an arbitrary third body. The equilibrium condition is

$$\frac{n_e n_i}{n_{ns}} = K(T_e) \tag{5}$$

in which $n_i$ is the number density of ions, and $n_{ns}$ is the number density of the seed neutrals. The equilibrium constant K is evaluated at the electron temperature.

Let the original number density of seed particles be $n_s$.

Then

$$n_s = n_{ns} + n_i \tag{6}$$

The degree of ionization of the seed material is defined by

$$\phi = n_e/n_s \tag{7}$$

For single ionization, $n_e = n_i$, and the above relations can be combined to give

$$\frac{n_s \phi^2}{1 - \phi} = K(T_e) \tag{8}$$

The number density of the seed material is expressed in terms of the seed fraction, S, defined as the mass of seed divided by the total system mass

$$S = \frac{n_s M_s}{n_s M_s + n_A M_A} \tag{9}$$

in which

$M_S$ = molecular weight of seed material

$M_A$ = molecular weight of base material

$n_A$ = number density of base gas particles

An additional parameter is the ratio of number densities (Ref. 13)

$$C_A = n_A/n_s \tag{10}$$

Using Eq. (9), this may be written

$$C_A = \frac{M_s}{M_A} \frac{1-S}{S} \tag{11}$$

The pressure of the mixture is

$$\begin{aligned} P &= \sum n k T \\ &= (n_A + n_s) k T_A + n_e k T_e \end{aligned} \tag{12}$$

Using Eqs. (7) and (10) gives

$$n_s = \frac{P}{(C_A + 1) k T_A + \phi k T_e} \tag{13}$$

This is used in Eq. (8) to yield

$$\frac{\phi^2}{1-\phi} \equiv \frac{k T_A K(T_e)}{P} (C_A + 1 + \phi T_e/T_A)$$

Letting

$$X = k T_A K(T_e) \tag{14}$$

the solution for $\phi$ may be written

$$\phi = \frac{2(1 + C_A)}{\left(C_A + 1 - \frac{T_e}{T_A}\right) + \sqrt{\left(C_A + 1 - \frac{T_e}{T_A}\right)^2 + 4\left(\frac{P}{X} + \frac{T_e}{T_A}\right)(1 + C_A)}} \tag{15}$$

The equilibrium constant is given by

$$K(T_e) = \left(\frac{2\pi m_e k T_e}{h^2}\right)^{3/2} e^{-I_p/k T_e} \tag{16}$$

in which

h = Planck's constant = $6.625 \times 10^{-34}$ joule-sec

$I_p$ = ioniation potential

Using this, X can be expressed as

$$X(\text{atm}) = 3.287 \times 10^{-7} T_A T_e^{3/2} \exp(-50350/T_e) \tag{17}$$

in which the temperatures are in °K.

The number density of electrons is then

$$n_e = \phi n_s$$

$$= \frac{\phi P}{k T_A} \quad \frac{1}{C_A + 1 + \phi T_e/T_A} \tag{18}$$

### 2.1.2 Collision Cross Sections

In Eq. (4), the summation is taken of the product of a number density and a collision cross section. For simplicity, this summation may be written as the sum of two terms, one for the neutrals, and one for the ions.

$$\sum_k n_k Q_{ek} = n_n Q_{en} + n_i Q_{ei} \tag{19}$$

in which $Q_{en}$ is an effective value for all neutrals. In the calculations, the electron-neutral cross section was taken as constant at $10^{-19}$ $m^2$. Figure 3 of Ref. 13 shows that experimental data for nitrogen cover a range of from $2 \times 10^{-20}$ to $12 \times 10^{-20}$, so that the variations in cross-section with temperature are of minor importance.

The expression for the conductivity can now be written:

$$\sigma = \frac{0.532\, e^2}{(m_e k T_e)^{1/2}} \left( \frac{n_n}{n_e} Q_{en} - Q_{ei} \right)^{-1} \tag{20}$$

The number density of neutrals is the sum of that of the base gas plus that of the nonionized neutrals

$$n_n = n_A + n_{ns}$$

Using Eqs. (6), (7), and (10) gives

$$\frac{n_n}{n_e} = \frac{1}{\phi} (C_A + 1 - \phi) \tag{21}$$

The electron-ion cross section is taken as the Spitzer value (Ref. 14)

$$Q_{ei} = \frac{0.9\, e^4}{(4\pi\epsilon_o k T_e)^2} \ln \left\{ \frac{12\pi}{e^3} \left[ \frac{(\epsilon_o k T_e)^3}{2 n_e} \right] \right\}^{1/2} \tag{22}$$

in which

$\epsilon_o$ = permittivity of free space

$\approx 10^{-9}/36\pi$ farad/m

Combining the above relations and evaluating the constants gives

$$\sigma = \frac{3.86 \times 10^{7}}{\sqrt{T_e}} \left[ \frac{n_n}{n_e} - \frac{2.52 \times 10^{9}}{T_e^{2}} \ell_n \left( 1.45 \times 10^{-7} \left\{ \frac{T_e^{3} T_A}{2P\phi} \left( 1 + C_A + \frac{T_e}{T_A} \phi \right) \right\}^{1/2} \right) \right]^{-1} \tag{23}$$

in which $\sigma$ is in mho/meter, the temperatures in degrees Kelvin, and the pressure P is in atmospheres. The solution for $\phi$ is given by Eq. (15) and $n_n/n_e$ by Eq. (21).

### 2.1.3 Electron Energy Loss Parameter

The electron collision energy loss parameter $\delta_k$ is very important. Unfortuntely, there is little agreement on a correct value. Argyropoulos and Demetriades (Ref. 3) have suggested that there is little variation in $\delta$ for $T_A$ between 2000 and 8000°K. Reference 3 uses the values of Ginzburg et al. (Ref. 15) of 394 for $O_2$ and 18.5 for $N_2$. Templemeyer et al. (Ref. 7) found a value of 100 for $N_2$ led to results in reasonable agreement with their experimental data. For the calculations here, a value of $\delta$ for nitrogen of 100 was used. The value of $\delta$ for air using the values given in Ref. 15 is

$$\delta_{air} \approx 0.7\,\delta_{N_2} - 0.3\,\delta_{O_2}$$

$$\approx 115$$

Based upon the results of Templemeyer, the value of $\delta$ for air was increased to 400 for the calculations. It should be noted that a high value of $\delta$ leads to a smaller value of the electron temperature.

In view of the uncertainty of the value of $\delta$, no attempt was made to include the losses from collisions with ions. Equation (3) then simplifies to

$$\frac{J^2}{\sigma} = 4k(T_e - T_A) n_e \sqrt{\frac{2k\,T_e\,m_e}{\pi}} \frac{\delta\, n_A}{m_A} (10^{-19}) \tag{24}$$

The mass of the molecule can be expressed in terms of the molecular weight by

$$m_A = M_A/6.03 \times 10^{26}\ \text{Kg}$$

With these values

$$J^2 = 9.431 \times 10^{-42}\, \sigma\delta(T_e - T_A) \sqrt{T_e}\, n_e n_A/M_A \tag{25}$$

Equations (23) and (25) are the two basic equations. They relate the conductivity, current density, and electron temperature. They have been solved numerically for scalar conductivity as a function of current density, gas temperature, and pressure.

#### 2.1.4 Results of Calculations

Results of the conductivity calculations are presented in Figs. 2 through 4. The conditions are summarized in the table below.

| Gas | Seed Fraction, S | Pressure, $P_{atm}$ | Figure Number |
|---|---|---|---|
| Nitrogen | 0.001 | 1 | 2a |
| Nitrogen | 0.001 | 10 | 2b |
| Nitrogen | 0.01 | 1 | 3a |
| Nitrogen | 0.01 | 10 | 3b |
| Air | 0.001 | 0.45 | 4a |
| Air | 0.001 | 10 | 4b |

The current density values on the figures are in amp/cm$^2$, rather than amp/m$^2$, since the numerical values are more convenient.

A comparison of Figs. 2a and b suggests that for a given gas temperature, $T_A$, the conductivity is about the same for a given value of J/P. It can be shown from the basic equations that this should be expected. A reasonable approximation is to neglect the electron-ion collisions in evaluating the conductivity. Combining the resulting form of Eq. (4) with Eq. (24) gives

$$T_e - T_A = \text{const. } \delta J^2/n_A n_e \tag{26}$$

Since

$$n_A = P/k T_A$$

and

$$n_e \sim S \phi P/k T_A$$

this becomes

$$\phi(T_e - T_A) = \text{const. } \delta \frac{J^2}{P^2} \frac{T_A^2}{S} \tag{27}$$

Since $\phi$ is determined primarily by $T_e$, this states that the electron temperature and conductivity are functions of the gas temperature $T_A$ and J/P.

The effect of varying the seed fraction may be seen by comparing Fig. 2a with 3a and Fig. 2b with 3b. The effect is not as large as that predicted by the approximate analysis above, primarily because the degree of ionization, $\phi$, is dependent upon the seed fraction S.

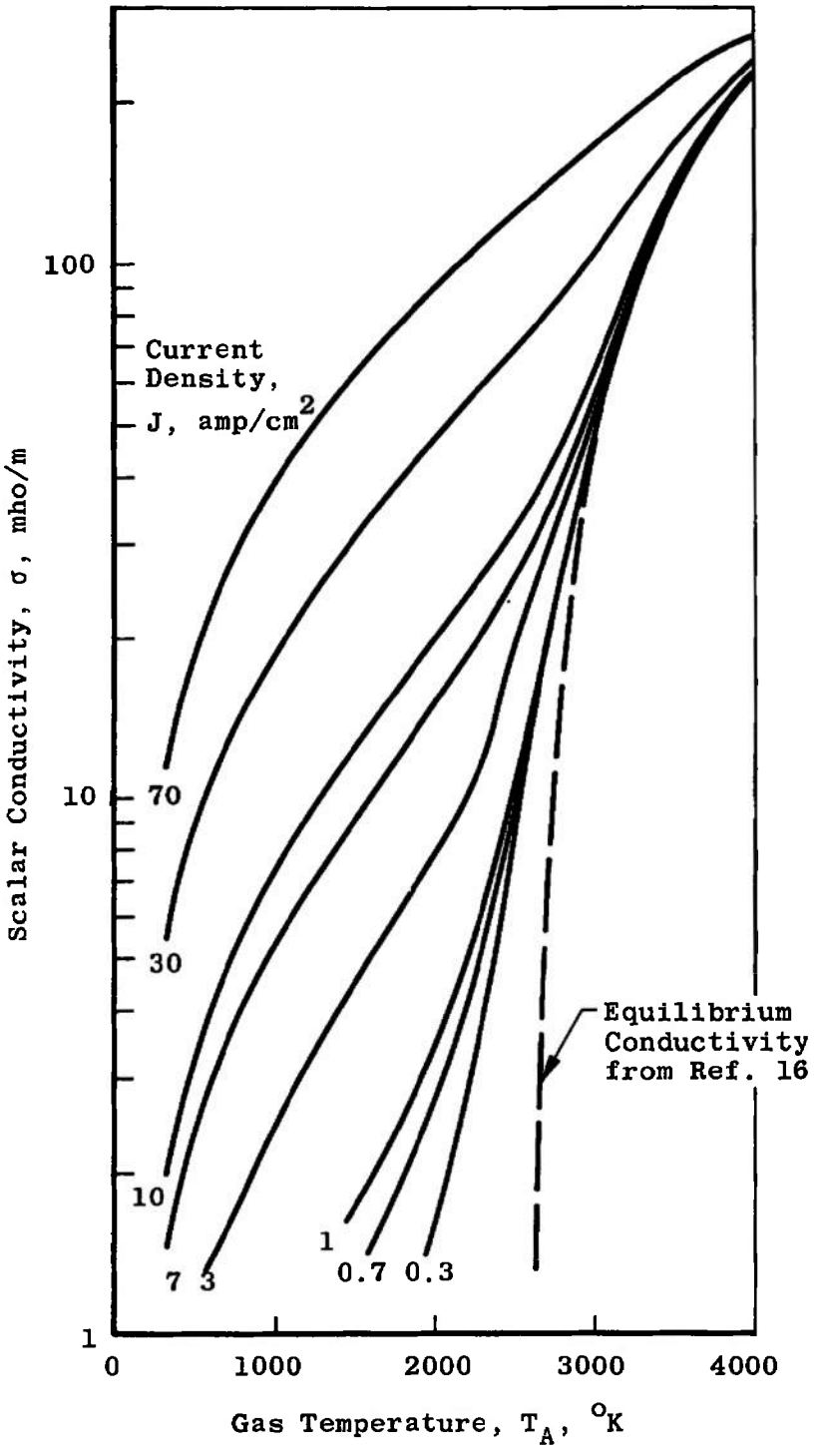


a. P = 1 atm

Fig. 2 Two-Temperature Conductivity of Nitrogen with Potassium Seed; S = 0.001

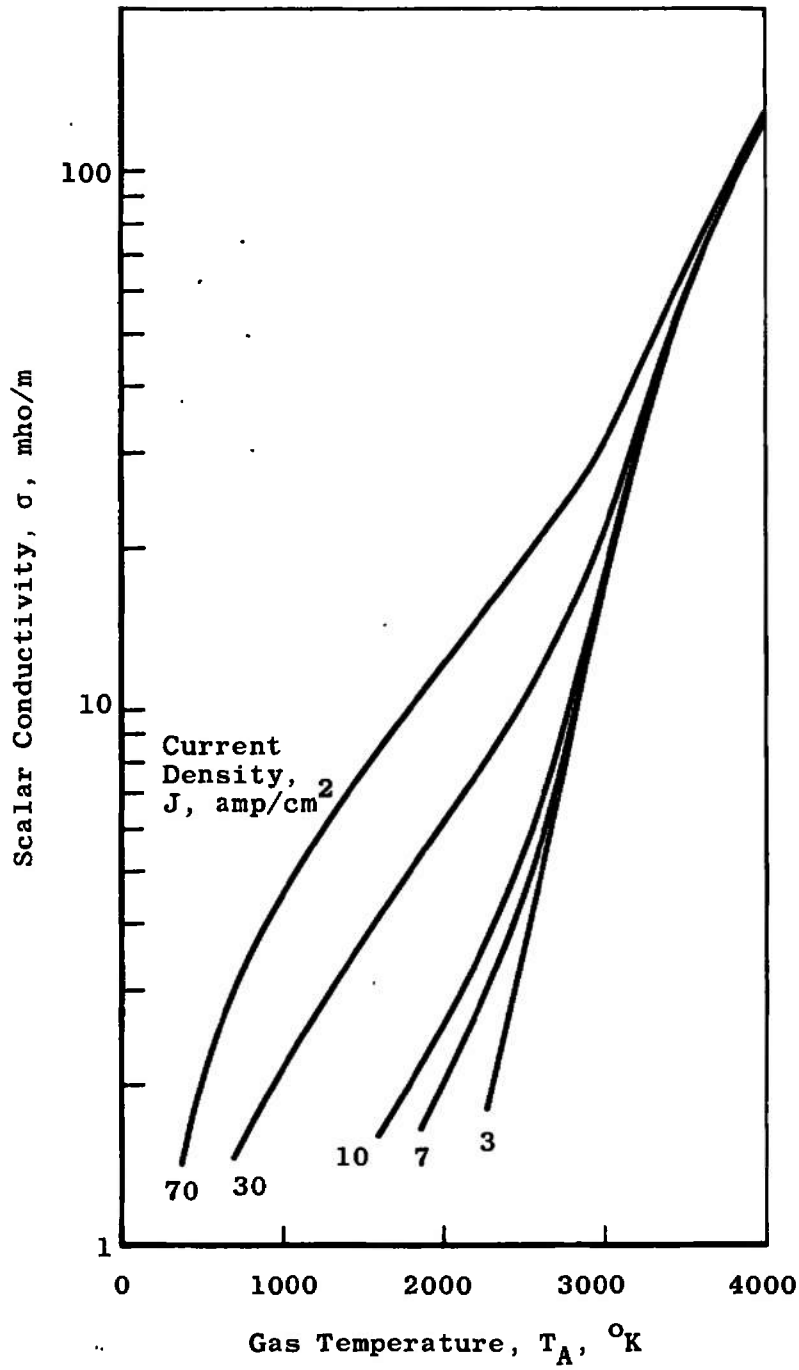


b. P = 10 atm

Fig. 2 Concluded

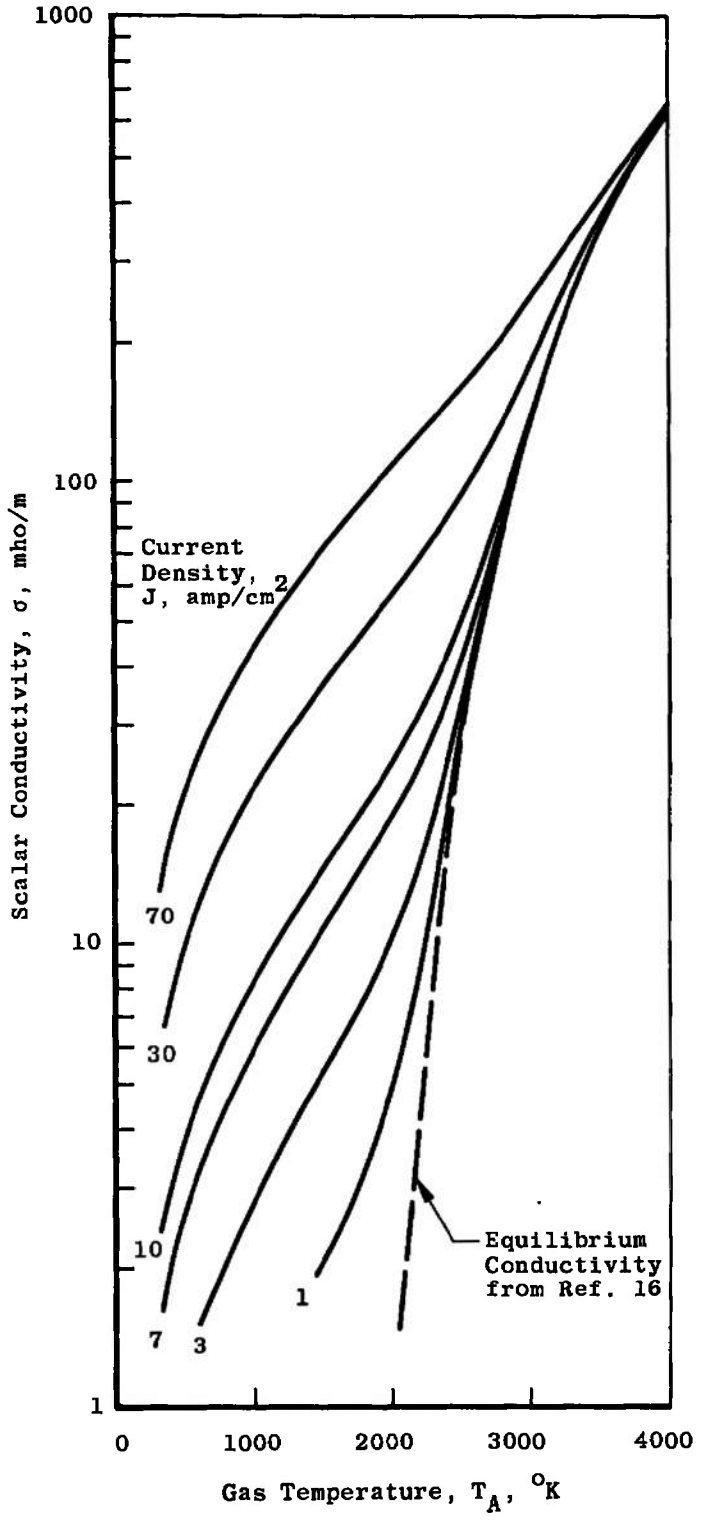


a. P = 1 atm

Fig. 3 Two-Temperature Conductivity of Nitrogen with Potassium Seed; S = 0.01

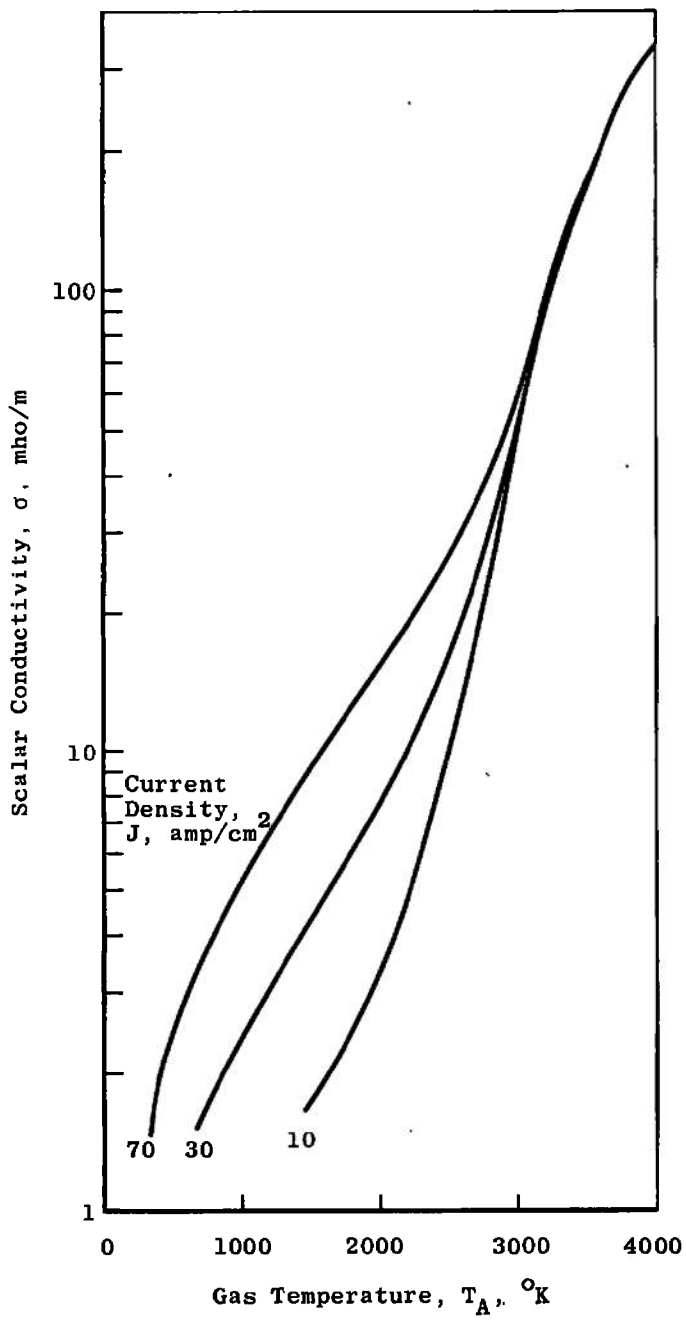


b. P = 10 atm

Fig. 3 Concluded

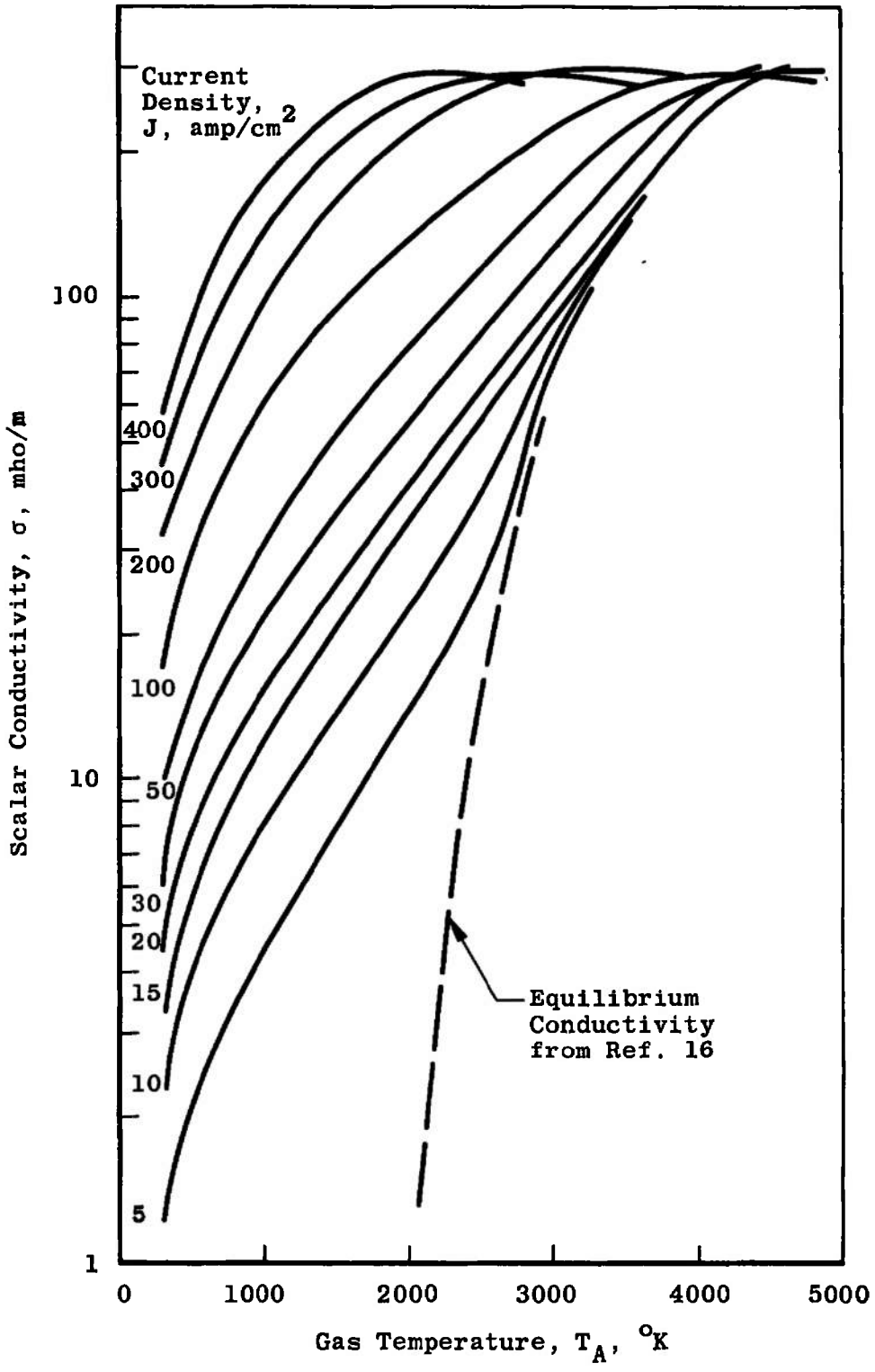


a. P = 0.45 atm

Fig. 4 Two-Temperature Conductivity of Air with Potassium Seed; S = 0.001

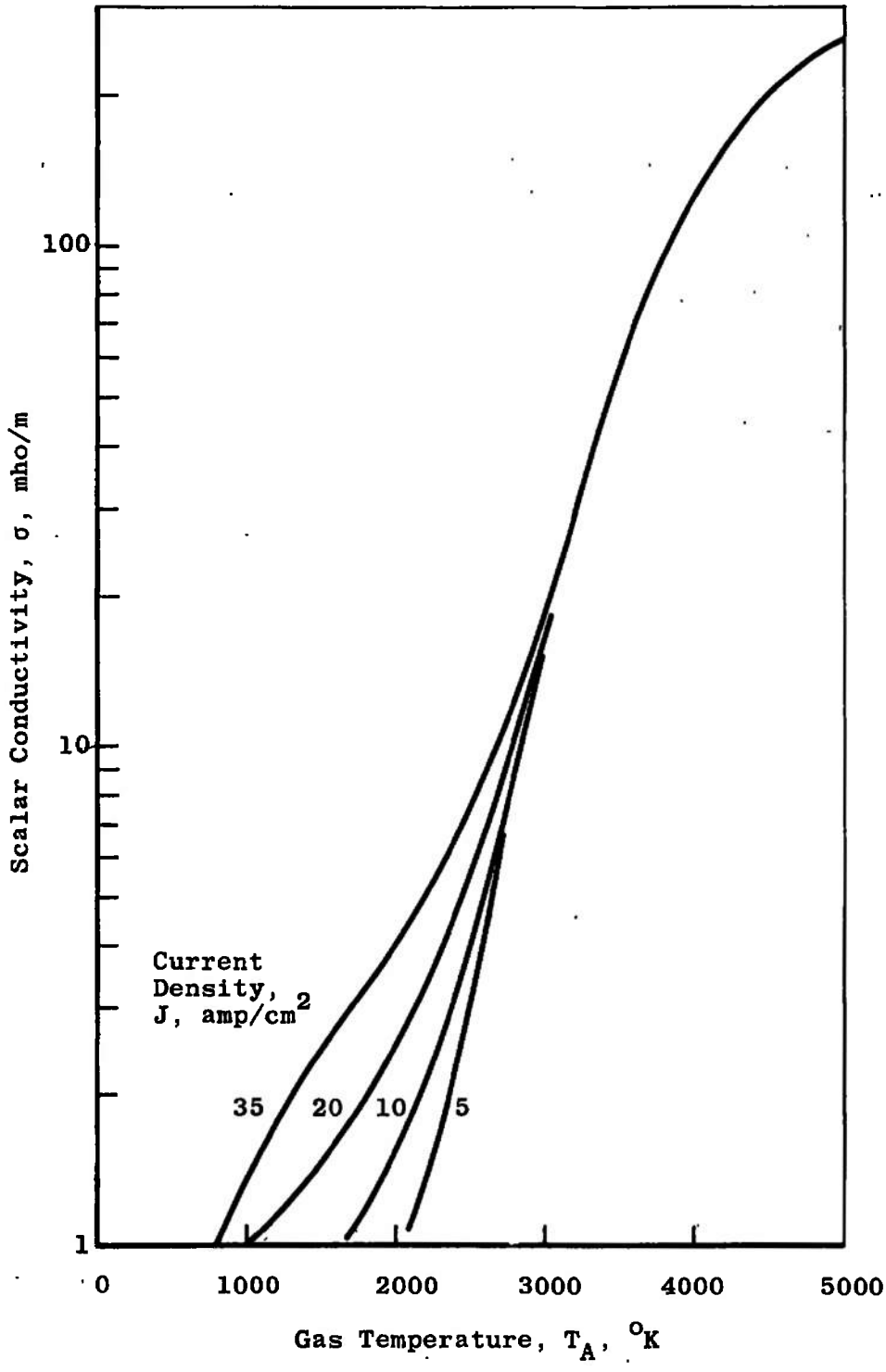


b. P = 10 atm

Fig. 4 Concluded

Comparing Figs. 2b and 4b gives the effect of the different values of the collision loss parameter, $\delta$. The higher values of $\delta$ for air give lower values of the conductivity if other conditions are the same.

#### 2.1.5 Comparison with Equilibrium Conductivity Calculations

The equilibrium values of conductivity as computed by Whitehead (Ref. 16) using the method of Schkarofsky (Ref. 17) are also shown in Figs. 2 through 4. For conditions of zero current and higher gas temperatures, Whitehead's approach is more accurate than that used here. Comparison of the results of the two models indicates that the values of conductivity obtained by the model used here are satisfactory.

### 2.2 CALCULATION OF BOUNDARY-LAYER VOLTAGE DROPS

The conductivity model described above may be used to describe the conduction of current across the thermal boundary layer on the electrodes of an accelerator. For the purpose of making preliminary estimates, the current density through the boundary layer may be assumed constant, although actually there are nonuniformities in the current density distribution, attributable to a number of factors (Ref. 3). The conductivity at any location within the boundary layer is then known as a function of the local temperature, $T_A$, and the current density. The excess voltage drop, i. e., the additional voltage drop above that which would occur if the conductivity were equal to the free-stream conductivity, is (per unit boundary-layer thickness)

$$\Delta V_{BL} = \frac{J}{\delta} \int_0^{\delta} \left( \frac{1}{\sigma_{BL}} - \frac{1}{\sigma_\infty} \right) dy \tag{28}$$

In Eq. (28), $\sigma_\infty$ is the conductivity based on free-stream conditions and $\sigma_{BL}$ is the conductivity in the boundary layer. The conductivity in the boundary layer is determined as a function of the geometric coordinate by assuming a Crocco (Ref. 18) enthalpy distribution

$$h = h_w + (h_\infty - h_w) \frac{U}{U_\infty} - \frac{1}{2} U_\infty^2 \left( \frac{U}{U_\infty} \right) \left( 1 - \frac{U}{U_\infty} \right) \tag{29}$$

in which $\infty$ denotes free-stream conditions and w denotes wall conditions. Velocity variations corresponding to laminar and turbulent boundary layers were used in Eq. (29) to provide enthalpy and thus temperature variation through the boundary layer. For the laminar case, the velocity was assumed to follow the polynominal relationship*

*A more realistic representation is obtained by using a stretched coordinate, but the additional complication was not felt to be worthwhile in this study.

$$\frac{U}{U_\infty} = \frac{3}{2}\left(\frac{y}{\delta}\right) - \frac{1}{2}\left(\frac{y}{\delta}\right)^3 \tag{30}$$

whereas for the turbulent case, the velocity was assumed to follow the power law relationship

$$\frac{U}{U_\infty} = \left(\frac{y}{\delta}\right)^{1/7} \tag{31}$$

Calculations have been made of the excess voltage drop across the gas dynamic boundary layer for nitrogen and air at a free-stream velocity of 10,000 ft/sec and free-stream temperatures of 3000, 3500, and 4000°K. Typical results for the laminar boundary layer are given in Fig. 5 for nitrogen and Fig. 6 for air. Figure 5a gives results for a seed fraction of 0.001, and Fig. 5b gives results for a seed fraction of 0.01. Comparison of these two shows only a minor effect of seed fraction.

At pressures of about an atmosphere and above, the excess voltage drop is nearly a linear function of the pressure. The data have been fitted with the relation

$$\Delta V_{BL}\ (v/cm) = V_1\,[P(atm)]^{0.965} \tag{32}$$

$V_1$ is the excess voltage drop at a pressure of 1 atm. Values of this parameter are given in Figs. 7 and 8 for free-stream temperatures of 3000, 3500, and 4000°K and a range of current densities. The effects of free-stream temperatures and seed fractions are surprisingly small. There are significant differences between the results for nitrogen and those for air.

The results of the calculation of the excess boundary-layer voltage drops for the turbulent velocity profile are given in Table I of Appendix I. There are a number of interesting trends to be noted. The excess voltage drop is seen to increase with increasing current density and increasing pressure. The drop is approximately proportional to the square root of the pressure for pressures above 1 atm. At lower pressures, the drop in air is greater than that in nitrogen, whereas at higher pressures the situation is reversed. No attempt was made to establish these trends on a more quantitative basis, since the magnitudes of the drops are generally quite small.

These results allow estimates to be made for the excess voltage drop on the E-field walls attributable to the gas dynamic laminar boundary layer. For turbulent boundary layers under the conditions investigated, the excess voltage drop was small.

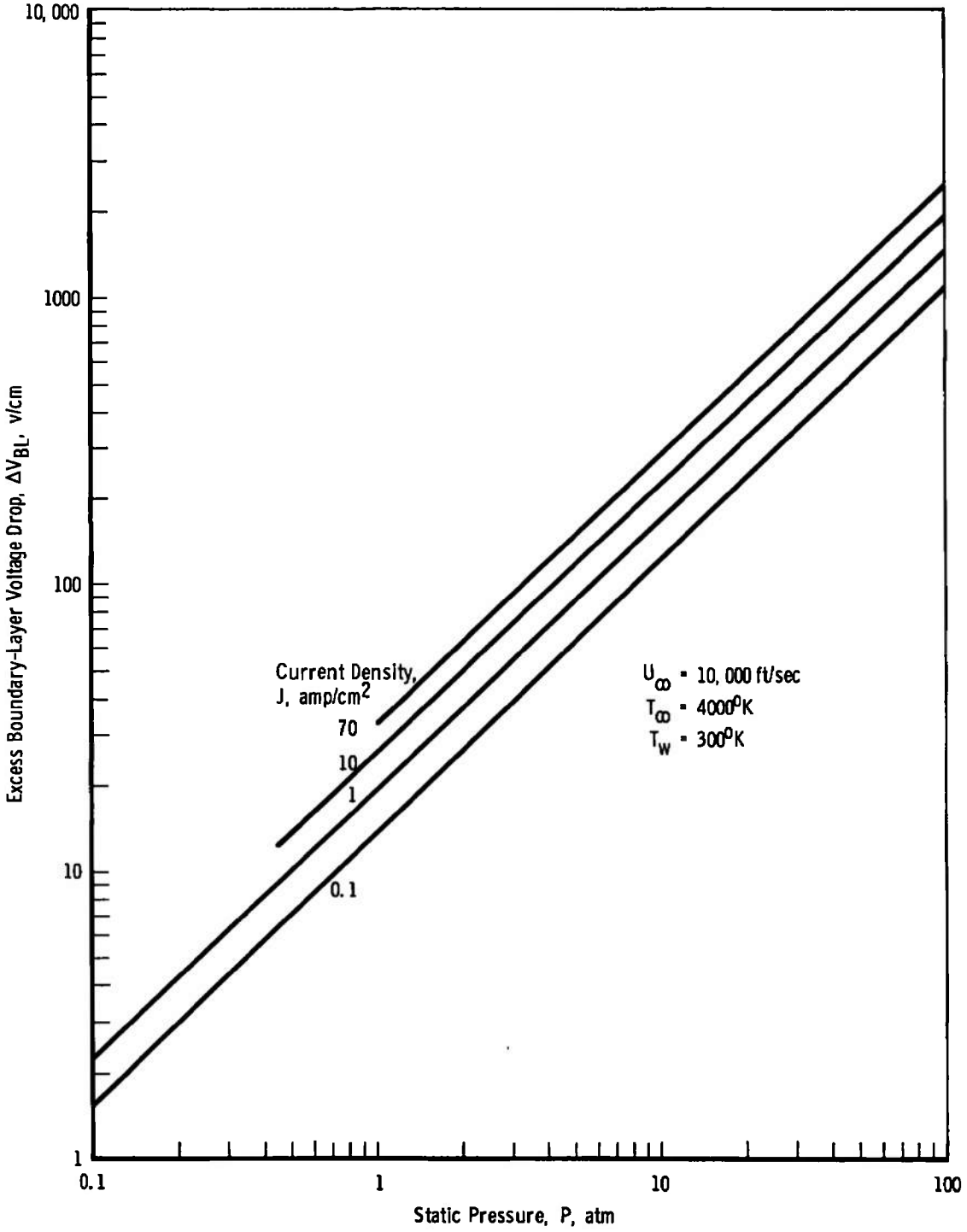


a. S = 0.001 Potassium

**Fig. 5 Excess Boundary-Layer Voltage Drop in Nitrogen for a Laminar Boundary Layer**

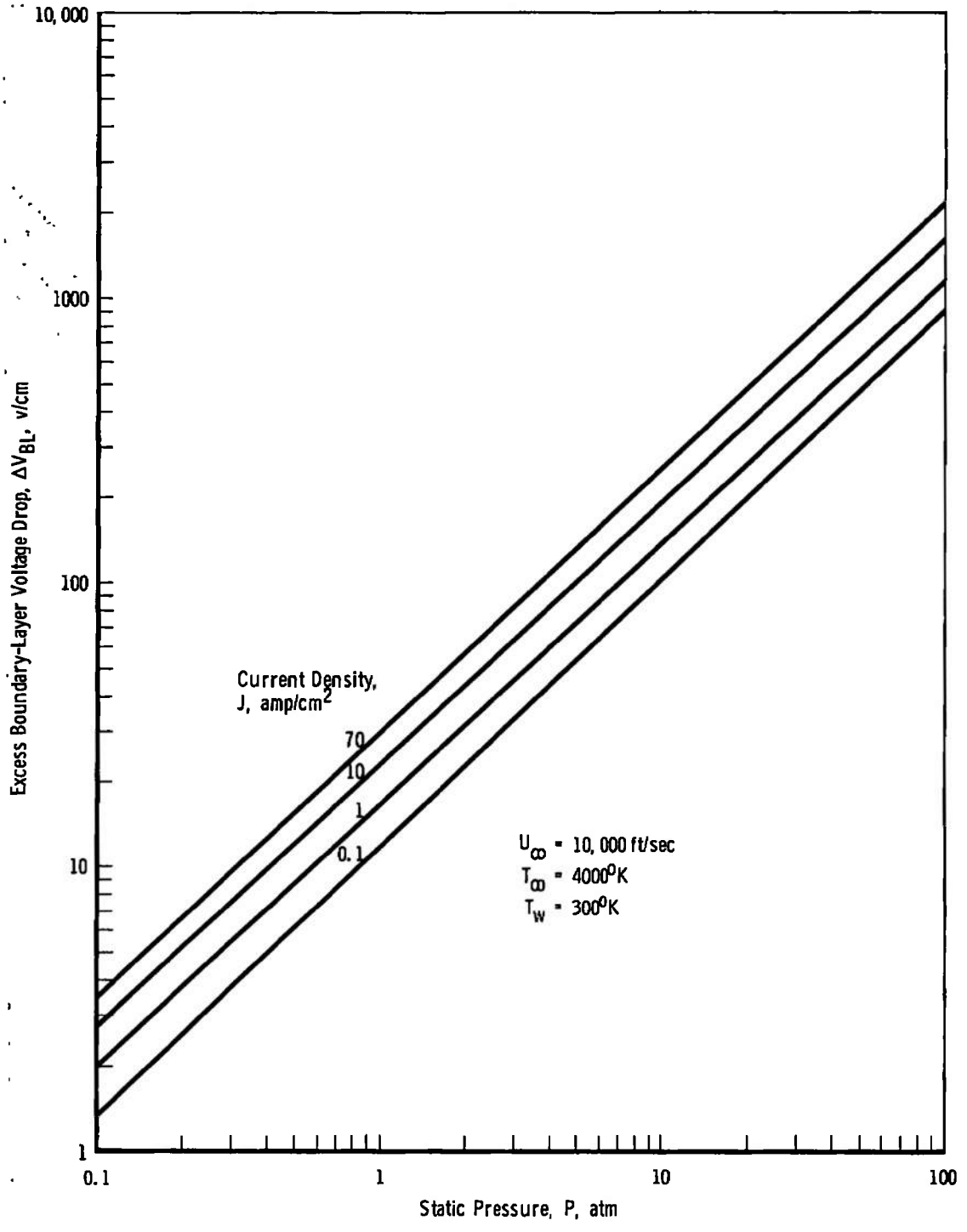


b. S = 0.01 Potassium

Fig. 5 Concluded

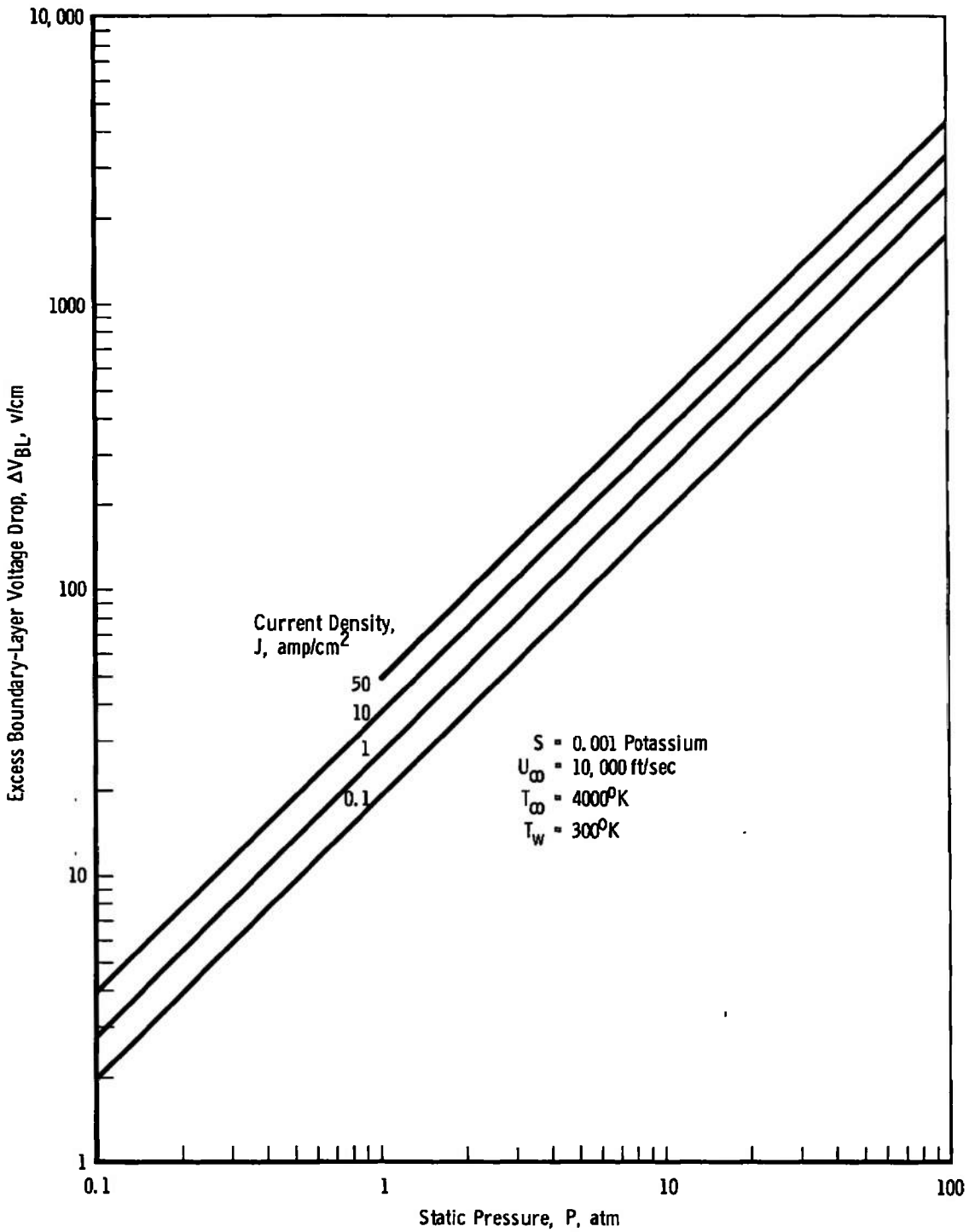


**Fig. 6 Excess Boundary-Layer Voltage Drop in Air for a Laminar Boundary Layer**

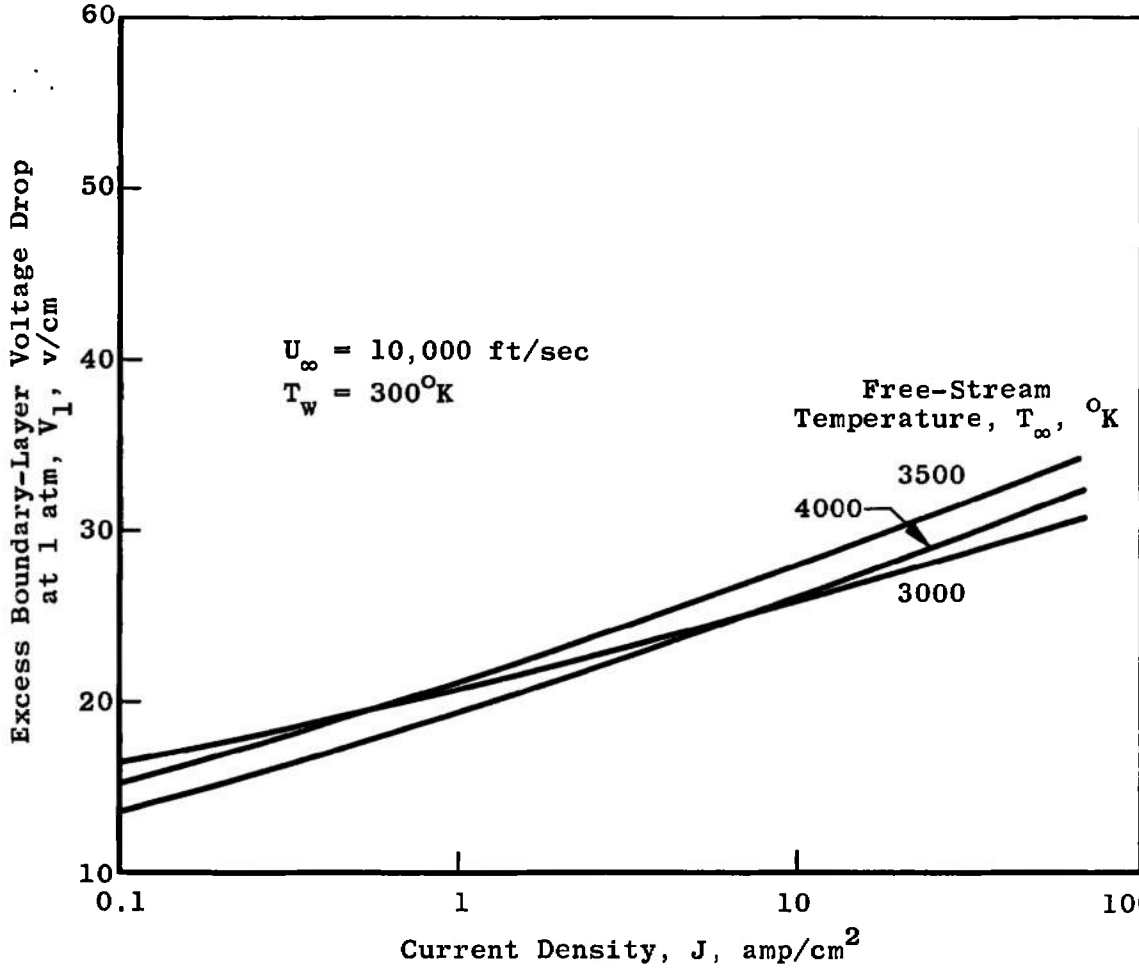


a. S = 0.001 Potassium

Fig. 7 Excess Boundary-Layer Voltage Drop at 1 atm in Nitrogen for a Laminar Boundary Layer

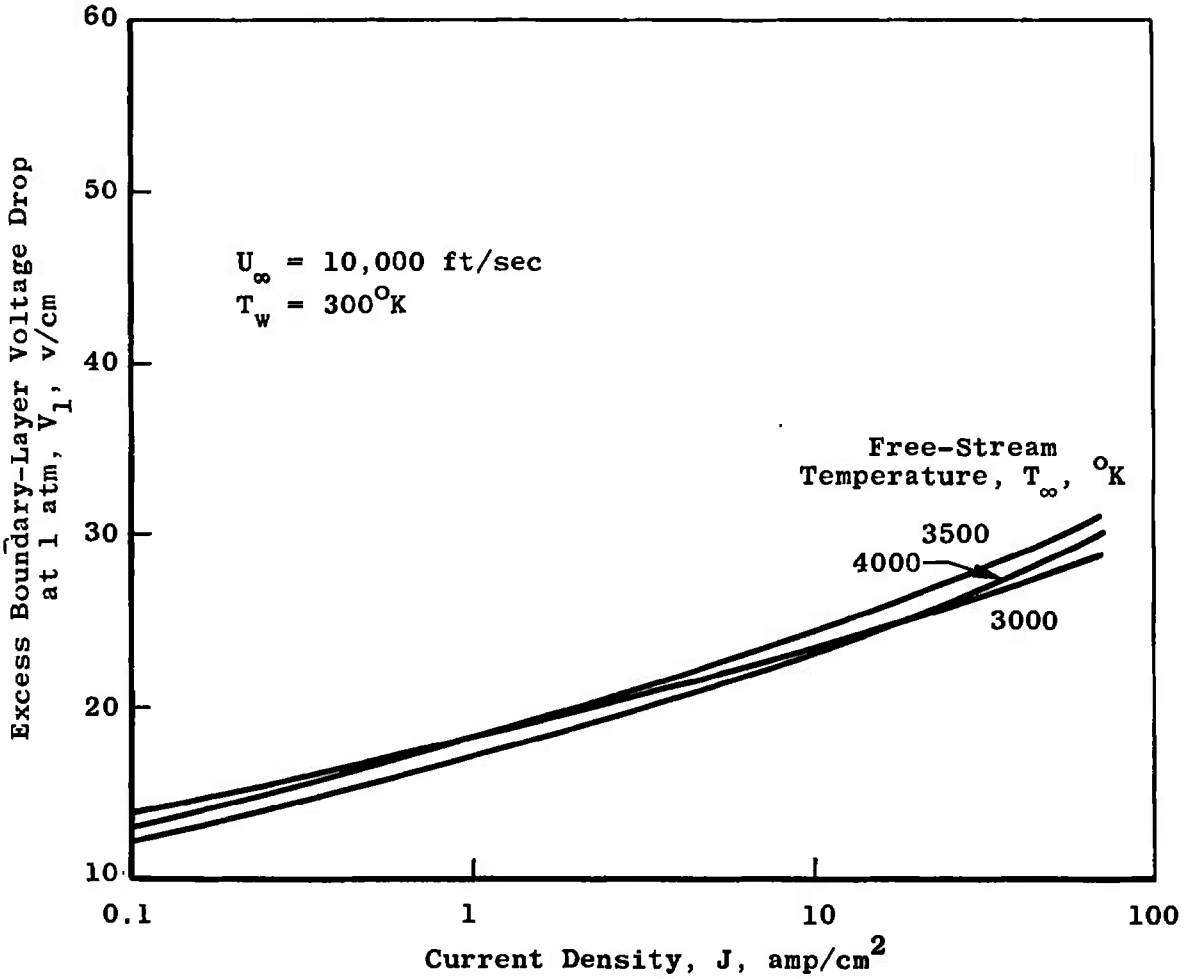


b. S = 0.01 Potassium

Fig. 7 Concluded

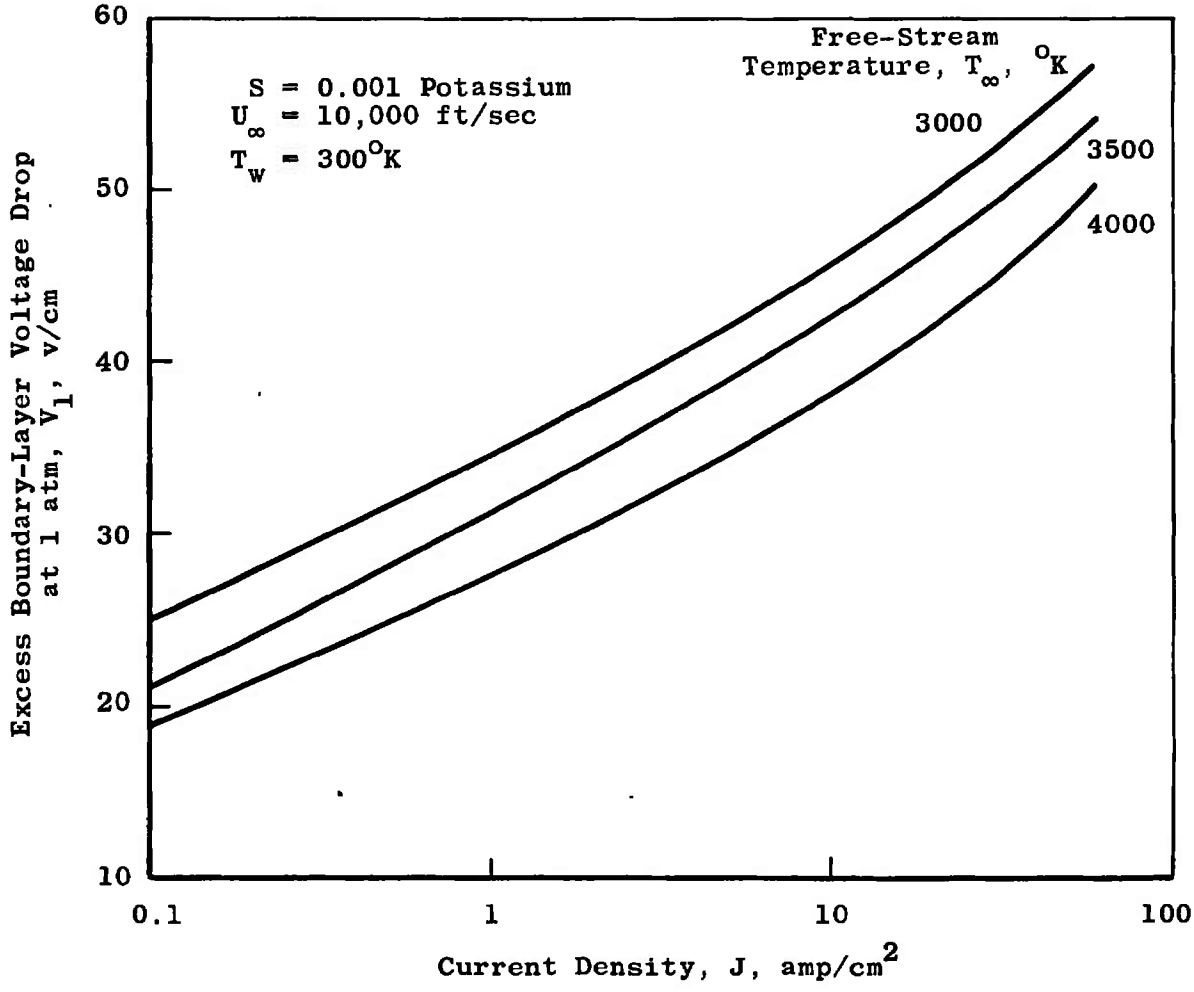


Fig. 8 Excess Boundary-Layer Voltage Drop at 1 atm in Air for a Laminar Boundary Layer

## SECTION III
## EXPERIMENTAL STUDY

The experimental study was undertaken in order to provide information on the boundary layer and sheath voltage drops in air with potassium seed. Previous studies have been made in argon (Refs. 4, 5, and 6), in seeded nitrogen (Ref. 7), and in unseeded air (Ref. 19). For monotonic gases, the collision loss parameter, $\delta$, is much less than for diatomic gases, so that the tests in argon are not applicable. The tests in seeded nitrogen are more appropriate, but the $\delta$ factor in air is sufficiently larger than in nitrogen that a separate test was felt worthwhile.

The conditions for the test were chosen to correspond to conditions anticipated for MHD accelerators. The tests were made in a shock tube, with the discharge taking place in the gas behind the incident shock. Although the boundary-layer thickness under these conditions is less than that expected in an accelerator, the predicted voltage drops were estimated to be large enough to be measurable.

### 3.1 APPARATUS

The experiments were performed in the VKF 40-mm shock tube (Ref. 20) (see Fig. 9). It is a pressure-driven shock tube, using helium at room temperature and pressures up to 15,000 psi in the driver. For these tests, the tube was modified to accept the fiber glass section shown in Fig. 10. In this section were located two diametrically opposed copper electrodes, each subtending 90 deg on the circumference, and five pins located in the sidewalls. The electrodes were 1 in. long, giving an area of $7.8 \times 10^{-4}$ $m^2$/electrode, and the sidewall pins were 0.049 in. in diameter. A nylon insert was used to insulate the electrodes from the metal portion of the tube. The electrodes were located 68 in. downstream of the diaphragm (Fig. 9).

The current was provided by capacitors, hooked up in a simulated transmission line, as shown in Fig. 11. This arrangement gives a fairly constant voltage at the electrodes. A typical waveform is shown in Fig. 11b. The capacitors are charged to an initial voltage $V_i$.

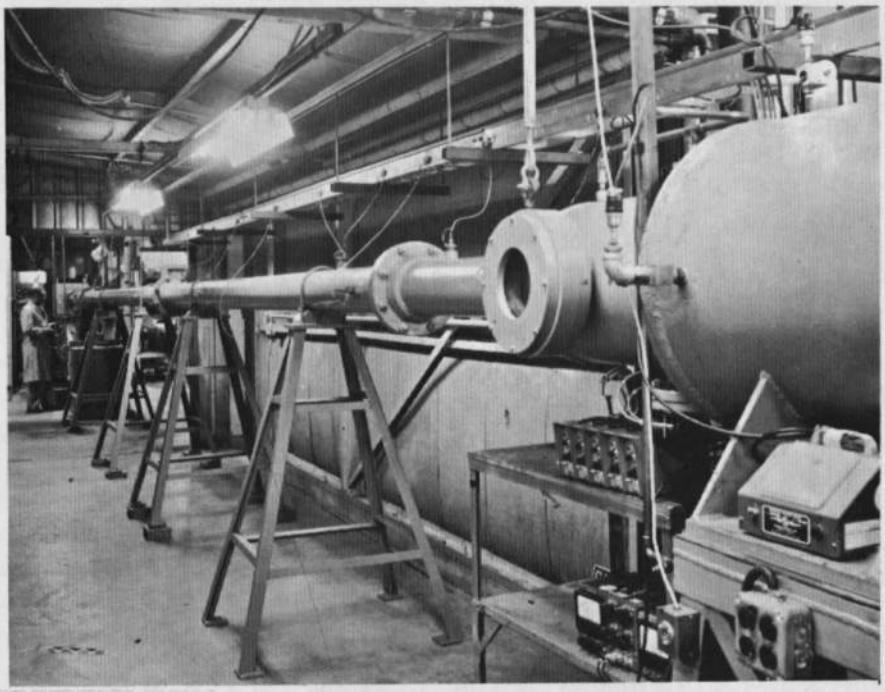

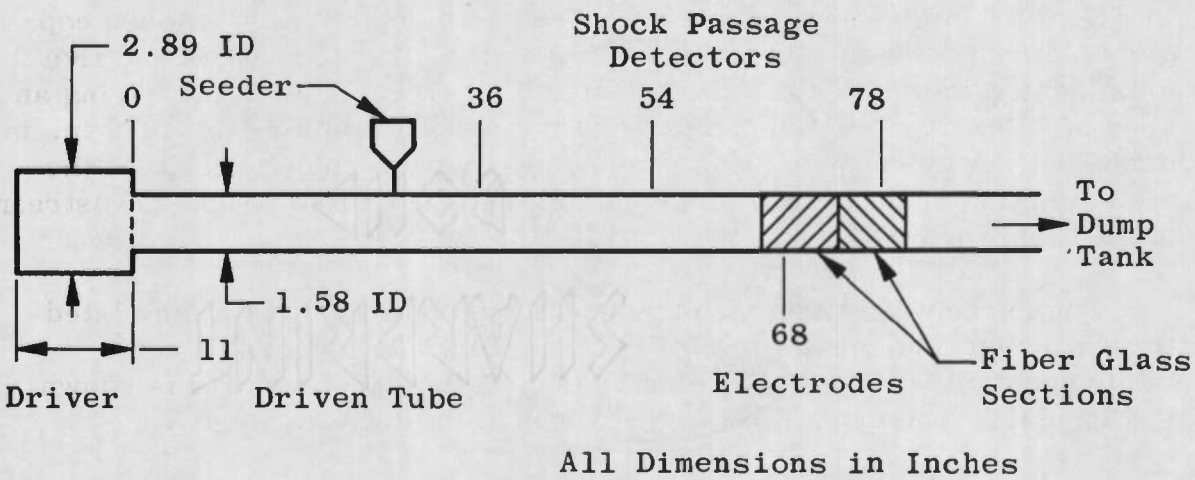


Fig. 9 AEDC-VKF 40-mm Shock Tube

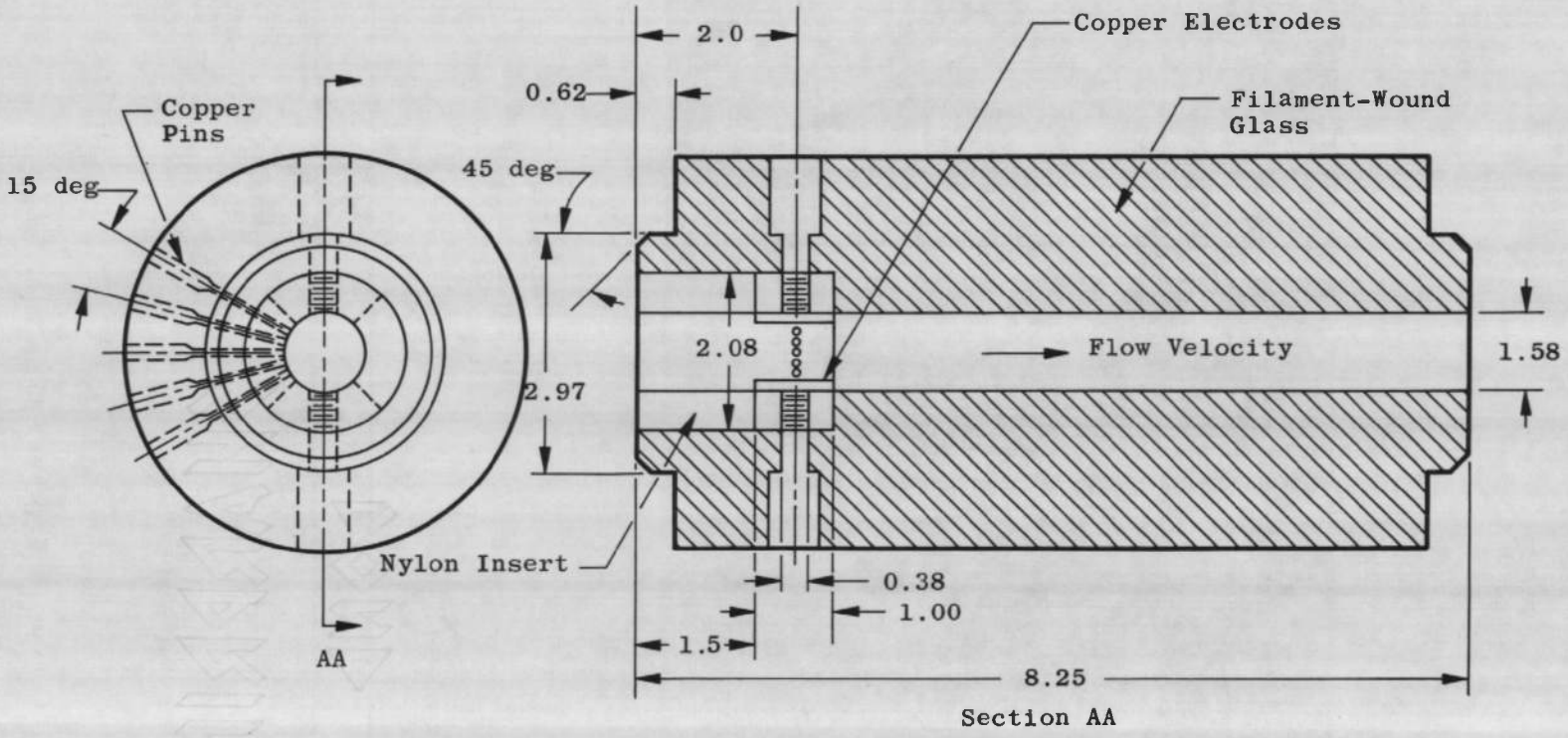


All Dimensions in Inches

Fig. 10 Fiber Glass Test Section Cross Section

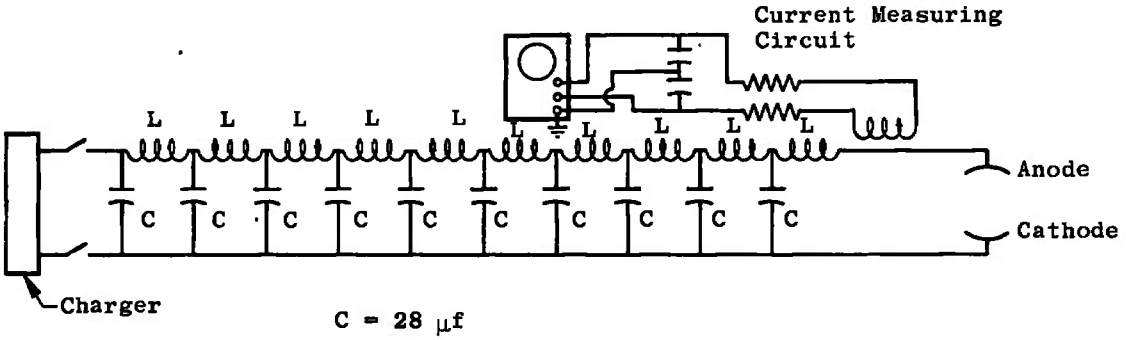


C = 28 μf
L = 25.5 μh
$Z_o$ = 0.953Ω
$t_d$ = 535 μsec
$t_r$ = 26.8 μsec

a. Schematic

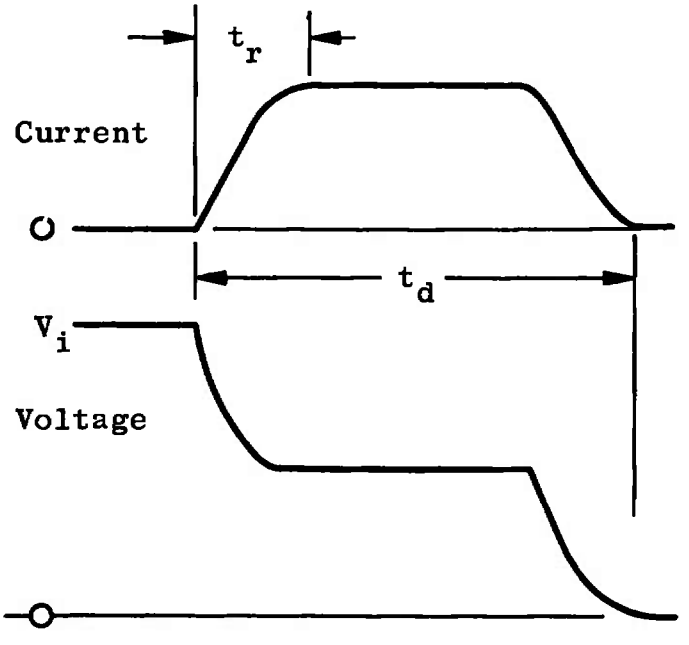


b. Ideal Discharge Characteristics

Fig. 11 Simulated Transmission Line Energy Supply

At the initiation of the discharge, the voltage decreases by an amount equal to the product of the current and the characteristic line impedance, $Z_o$. The voltage across the electrodes is therefore a function of the current or equivalently, the load resistance. The voltage remains constant for a period of time and then decreases. This particular transmission line had been set up for other tests and was not changed for these tests. The discharge time of 535 $\mu$sec was significantly longer than needed.

The capacitors were charged to an initial voltage of from 100 to 800 v, with 800 v being the maximum that could be applied without an arc-over. The discharge was initiated by the passage of the shock-heated gas.

The gas was seeded by using the centrifugal seeder technique developed by Smithson (Ref. 21). In this technique, the charge gas is brought into the tube through a bed of powdered potassium carbonate, which has been ground to a mean particle size of approximately 1 $\mu$. The seed material remains in suspension in the charge gas for a period of time. These seed particles settle toward the bottom of the tube with time, so that it is necessary to make the shot within approximately 1 min.

Measurements were made of the shock velocity, the initial pressure, and voltages on the electrodes and pins in the sidewalls.

### 3.2 SHOCK TUBE CONDITIONS

The shock tube conditions were chosen so that a reasonable value of the conductivity would be obtained. The seeding technique used in the present test was the same as used by Smithson (Ref. 21). Some of his results taken in the same tube are given in Fig. 12. His data were taken with a conductivity coil similar to that used by Lin, Resler, and Kantrowitz (Ref. 22). This device has the advantage that it is relatively free of complications because of the boundary layer. Smithson's results are denoted by squares for the unseeded runs and by circles for the seeded runs. In addition, a symbolism is used to denote the initial pressure. The open circles are values for runs with initial pressures of 0.075 psia, and these runs give low values for the conductivity. For higher initial pressures, the conductivity is somewhat higher and attains reasonable values. The reason for the falloff of conductivity with decreasing pressure is probably tied in with the way the seeder operates. At low pressures, it is possible that the seed particles are not carried into the tube adequately. There were some runs made at even lower initial pressures than shown in Fig. 12. For initial pressures of 0.038 psia, shock Mach numbers of from 9.6 to 10 were obtained, but the

conductivity was too low to be measured. The results indicate that the maximum conductivity was obtained with initial pressures of from 0.15 to 0.4 psia, at shock Mach numbers from 8.9 to 9.4. At lower initial pressures and higher shock strengths, the conductivity falls off because of the seeder, and at higher initial pressures, and lower Mach numbers, the conductivity decreases because of the reduced temperature. Some additional measurements of conductivity by the same technique were made during the present tests. These values are given in Fig. 12 by the diamond symbols, and the results are similar to those of Smithson.

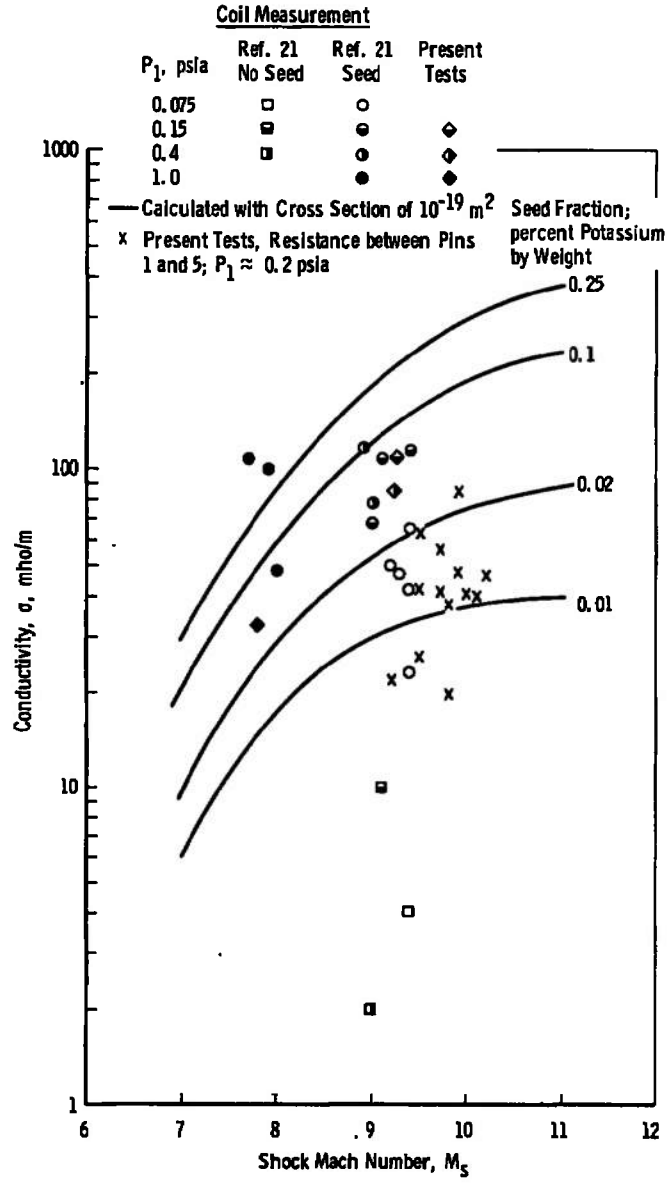


**Fig. 12 Experimental Conductivity of Seeded Air**

It was found during the present tests that at an initial pressure of 0.2 psia, higher shock Mach numbers were obtained than obtained by Smithson. The results are summarized in Fig. 13, plotted as shock Mach number versus the diaphragm pressure ratio, $P_4/P_1$. Smithson's values are denoted by the open circles. These values agree reasonably well with those predicted on the basis of the results of Glass and Hall (Ref. 23), with an adjustment for the difference in areas of the driver and the driven tube. Calculations were also made using real gas property data, but the results were identical to those obtained using ideal gas relations. Values obtained during the present tests are denoted by the closed circles. The values are generally higher than those of Smithson, except at the lower diaphragm pressure ratios. Shock Mach numbers of 10 were obtained with initial pressure ratios about 20 percent of those that Smithson found necessary.

A possible explanation for the differences could be in the diaphragm opening process. White (Ref. 24) has proposed a formation-by-compression model in which the diaphragm opening time is considered finite, and the shock wave is assumed to form from an isentropic compression field. The upper curve gives the predicted shock Mach numbers based upon this model. Slight differences in the calculated values were obtained using the two models for gas properties. There is no way of determining a priori whether the formation-by-compression model is applicable, but past experience has indicated that the formation-by-compression model is perhaps the correct one for unheated drivers at high values of the diaphragm pressure ratio. The results in Fig. 13 support this. At the lower pressure ratios, the experimental values of the shock Mach number agree with the lower curve, and the data seem to approach the upper curve at the higher values of the pressure ratio. The scatter that is evident at pressure ratios of about $7 \times 10^4$ could be because of the variation in the diaphragm opening process from run to run. It is not known why different results were obtained from the two series of tests, but it possibly could be because of a different manufacturing run of diaphragms.

The nominal initial pressure was selected as 0.2 psia (11 mm Hg). The conditions behind the incident shock are given in Fig. 14, as obtained from the charts of Ref. 25. The static temperature varies from 3500 to 3800°K, and the static pressure from 1.6 to 1.9 atm. Scalar conductivities are also shown. For 0.1-percent seed, the scalar conductivity is between 100 and 200 mho/m.

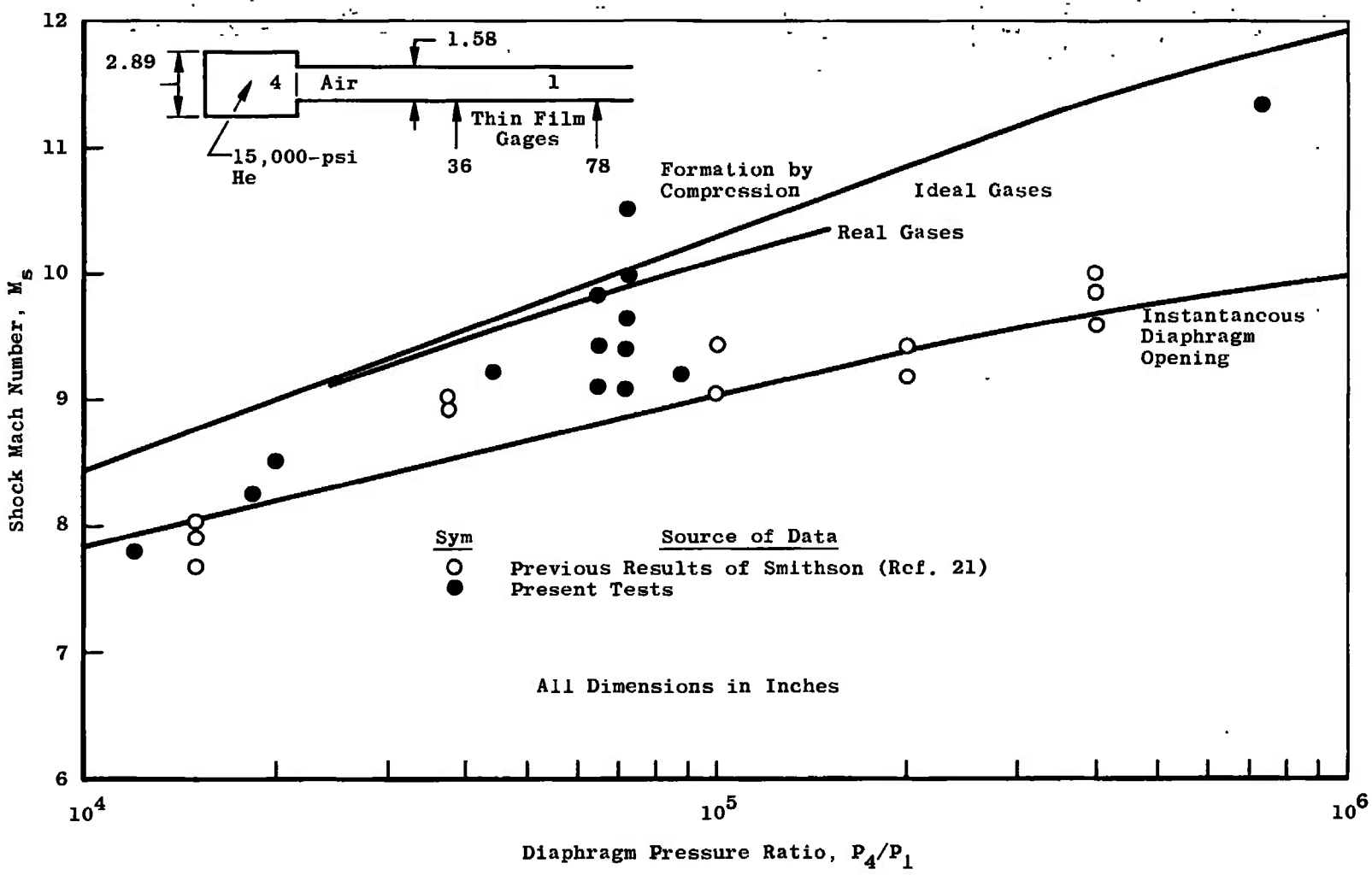


Fig. 13 Shock Mach Number versus Diaphragm Pressure Ratio for AEDC-VKF 40-mm Shock Tube

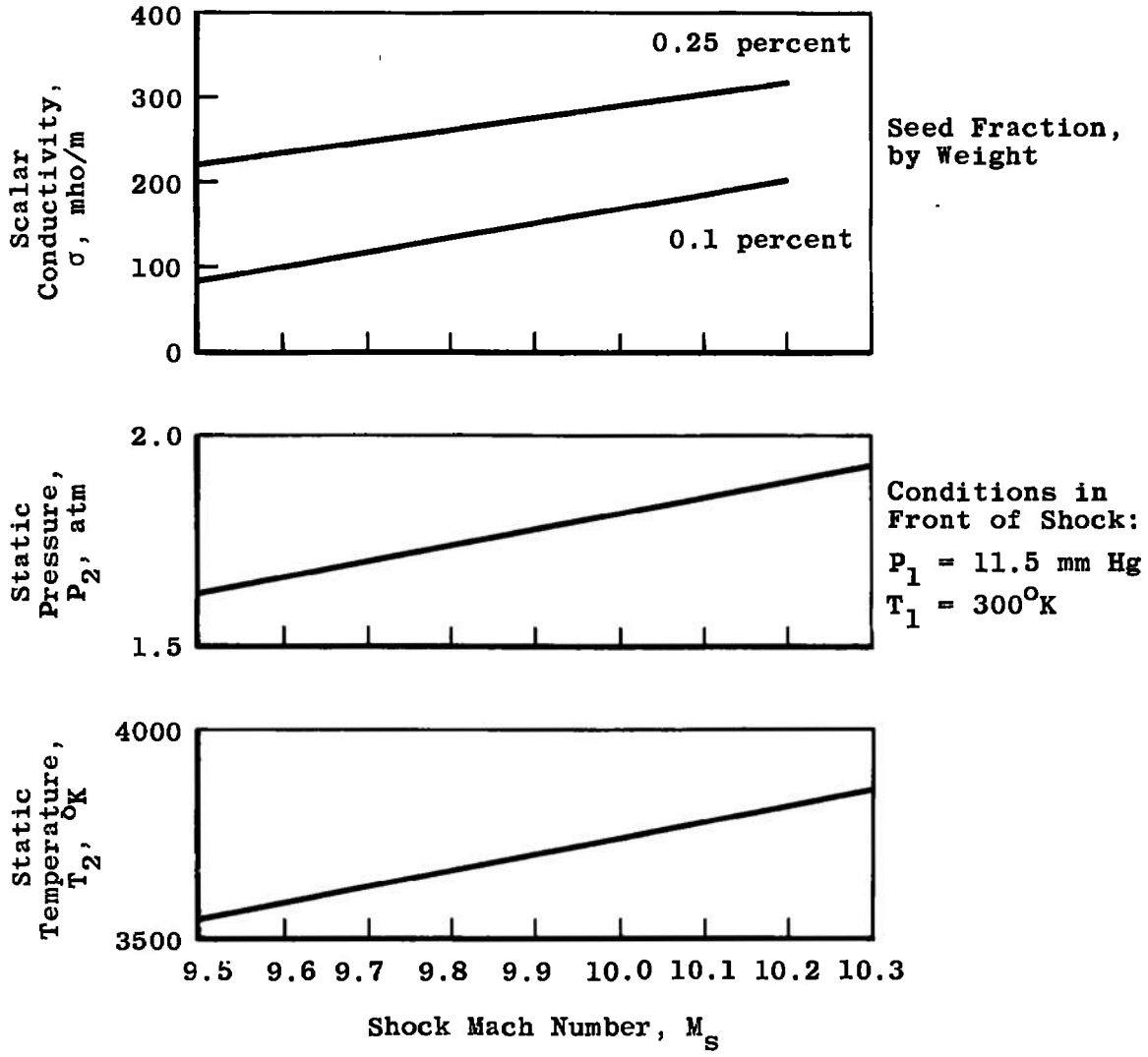


Fig. 14 Conditions behind an Incident Shock in Air

The state of the boundary layer behind the incident shock was estimated using results from other sources. The experimental results of Hartunian (Ref. 26), along with similar results obtained locally, indicate that there should be 69 $\mu$sec of laminar flow behind the incident shock. The results of Mirels (Ref. 27) lead to an estimate of a useable run time of 50 $\mu$sec, at which time the interface would arrive. Therefore, the boundary layer is assumed to be completely laminar.

Reliable estimates of the boundary-layer thickness are difficult to make. Using the results given by Mirels (Ref. 27), the laminar boundary-layer thickness 20 $\mu$sec after the shock has passed, at which time the electrical traces were read, is estimated to be 0.050 in. The calculated variation of the boundary-layer thickness at the electrodes with time is given in the lower part of Fig. 15. In the upper portion of Fig. 15, the calculated variation of the excess boundary-layer voltage (including both boundary layers) with time is given for a range of current densities. The current density range covered in these tests was from 3 to 40 amp/cm$^2$. The predicted total excess drop at 20 $\mu$sec is then from 12 to 20 v.

### 3.3 VOLTAGE DISTRIBUTION DATA

The potentials of the pins and the anode were recorded during the discharge. Initial charge voltages of 100, 200, 400, 600, and 800 v were used.

Considerable difficulty was encountered in measuring the pin potentials. It was necessary to employ compensating networks at the probes, as shown in Fig. 16, to compensate for the impedance of the probe and connecting cables. Otherwise, the delay time exceeded the useful run time. Other investigators (Refs. 4 and 6) have found it necessary to recess the pins to make sidewall voltage measurements in argon plasmas. For the present tests in seeded air, better results were obtained with the pins mounted flush.

Figure 17 gives typical electrical data obtained. Upon arrival of the shock wave and the initiation of the current flow, the voltage across the electrode decreases because of the voltage drop across the last inductor (Fig. 11). After approximately 20 $\mu$sec, the voltage starts rising, indicating an increase in the resistance. The reason for this rise is not clear, since it is apparently too early for interface arrival, and the boundary-layer voltage drop is not sufficiently large to cause such a large increase. The ringing afterwards is a characteristic of the transmission line. The middle trace gives voltage on Pin No. 1, and the

trace is similar to that of the electrode voltage, during the useful run time. There is an initial lag in the voltage, perhaps because of the capacitance of the measuring circuit. The current is given in the upper trace and points out a serious difficulty with interpreting the data. The rise time for the transmission line was 27 μsec, whereas the constant voltage time lasted only for about 20 μsec. The traces should be read at the time for which the current is not changing with time, in order to minimize the effects of inductance on voltage readings. Since this is not possible, the traces were read at 20 μsec, just before the voltage started to rise. Estimates of the inductance lead to the conclusion that the error is at most 10 percent in the voltage.

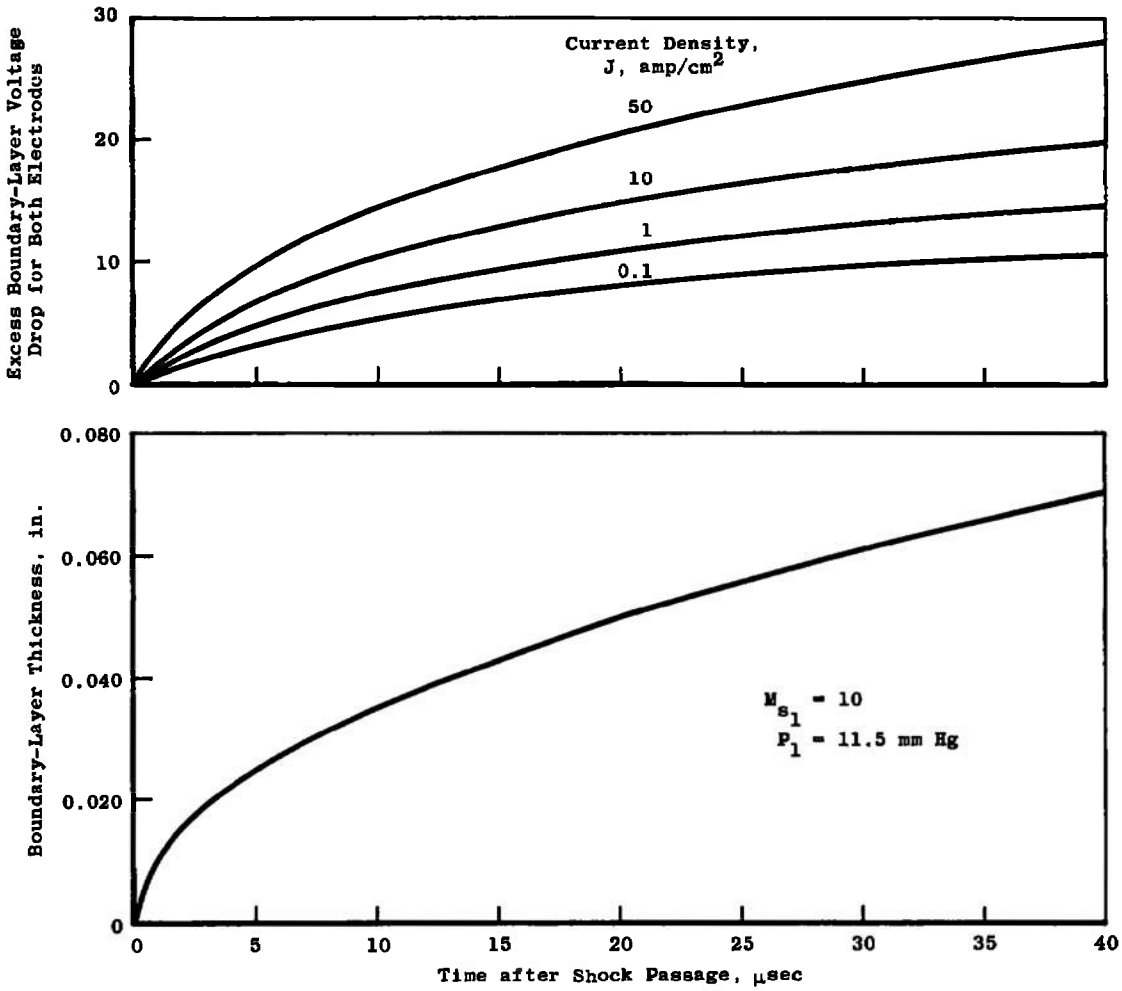


Fig. 15 Characterics of Boundary Layer behind the Incident Shock

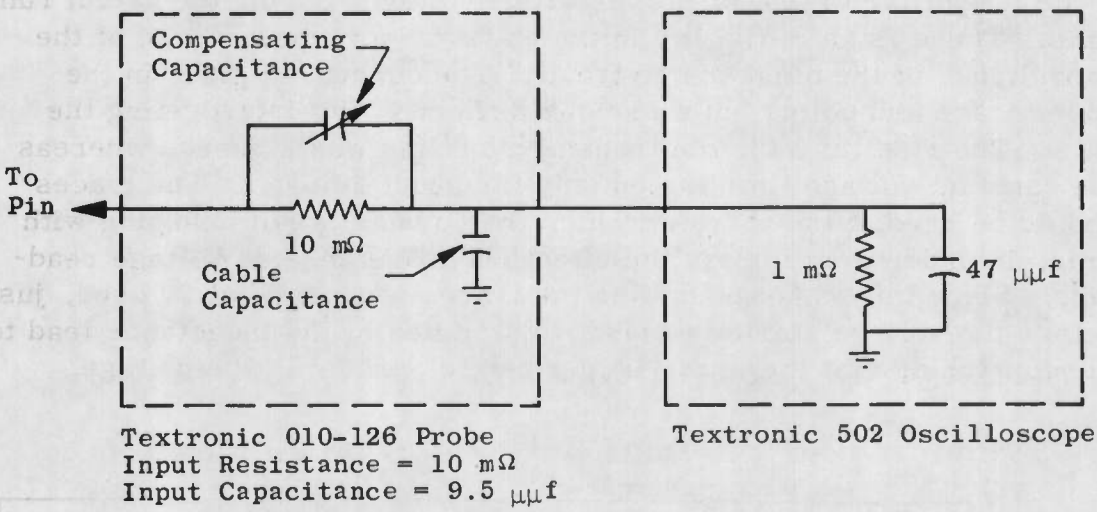


Fig. 16 Schematic of Probe-Scope Arrangement

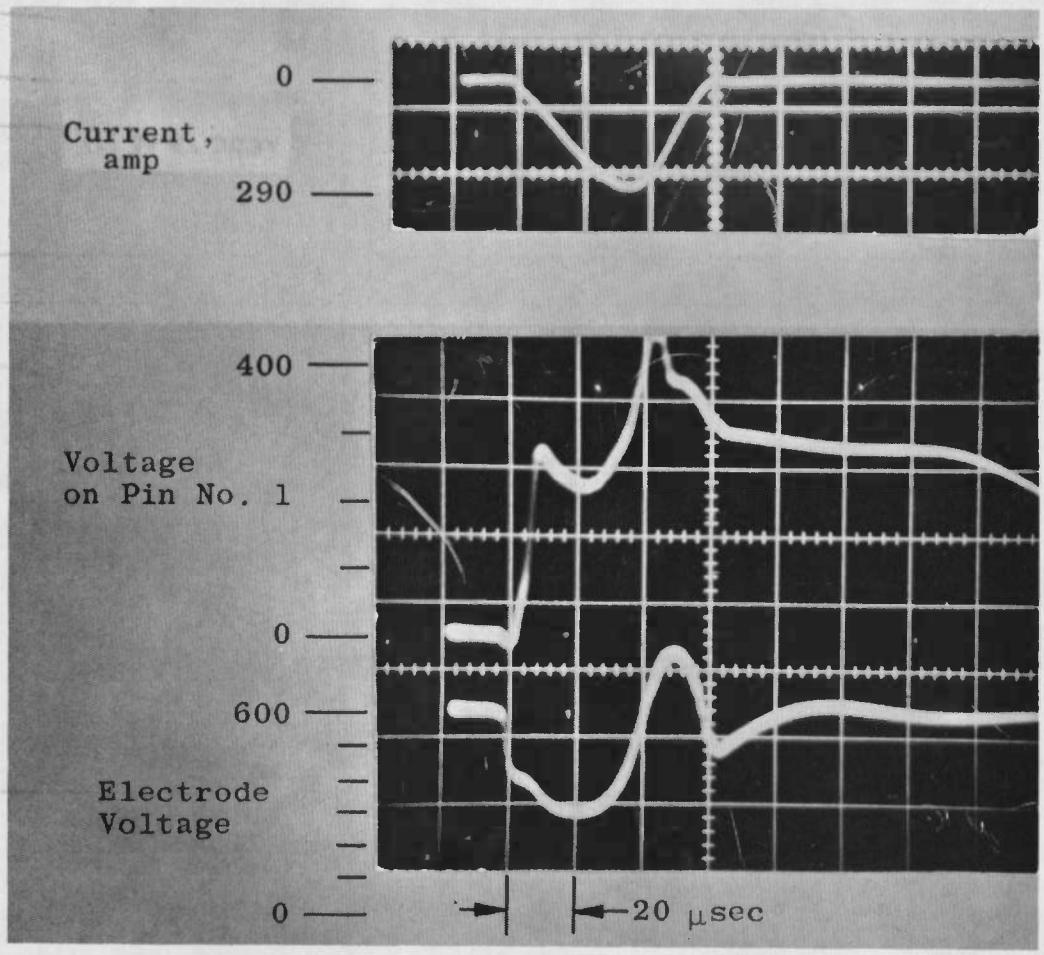


Fig. 17 Typical Oscilloscope Traces

Figure 18 gives the time variation of the various pin voltages, normalized with respect to the electrode voltage. The voltage ratios remain reasonably constant for a considerable length of time, even though the electrode voltage varies similarly to that in Fig. 17.

The traces were read at 20 $\mu$sec, and the values of the voltages are given in Table II. The data have been grouped according to the initial voltage.

### 3.4 DISCUSSION OF VOLTAGE DISTRIBUTION DATA

Interpretation of the results of the voltage distribution tests is made using the following assumptions:

a. The sidewall pin locations can be related to an effective distance for an equivalent rectangular channel.

b. The voltage drop across the channel can be divided into three separate parts: that attributable to the resistance of the uniform free stream, the excess voltage drop attributable to reduced conductivity in the thermal boundary layers, and the voltage drop associated with the electrode sheaths.

c. The current density across the channel is constant.

The circular geometry is, of course, inconvenient for the determination of voltage distributions, because of the nonuniform current conduction paths. The approach used here is to relate the circular geometry to an "equivalent" rectangular geometry. Using a conducting paper analog, equipotential lines for the circular geometry were obtained. The equipotential lines from the pin locations were then traced back to the center of the channel. These equipotential lines are shown in Fig. 19. Therefore, the measurements with the pins can be used to determine the potential distribution on the center. The electric field on the center can be related to the potential of the electrodes by using the results of Fishman (Ref. 28). The effective separation distance of the electrodes is found to be 0.865D for 90-deg electrodes. Therefore, the apparent electrode locations are as shown in Fig. 19. The width of the equivalent channel is also found from Fishman's results, using the results for the total channel resistance. It is found that for 90-deg electrodes, the effective channel is square. Therefore, the equivalent rectangular channel is as shown in Fig. 19.

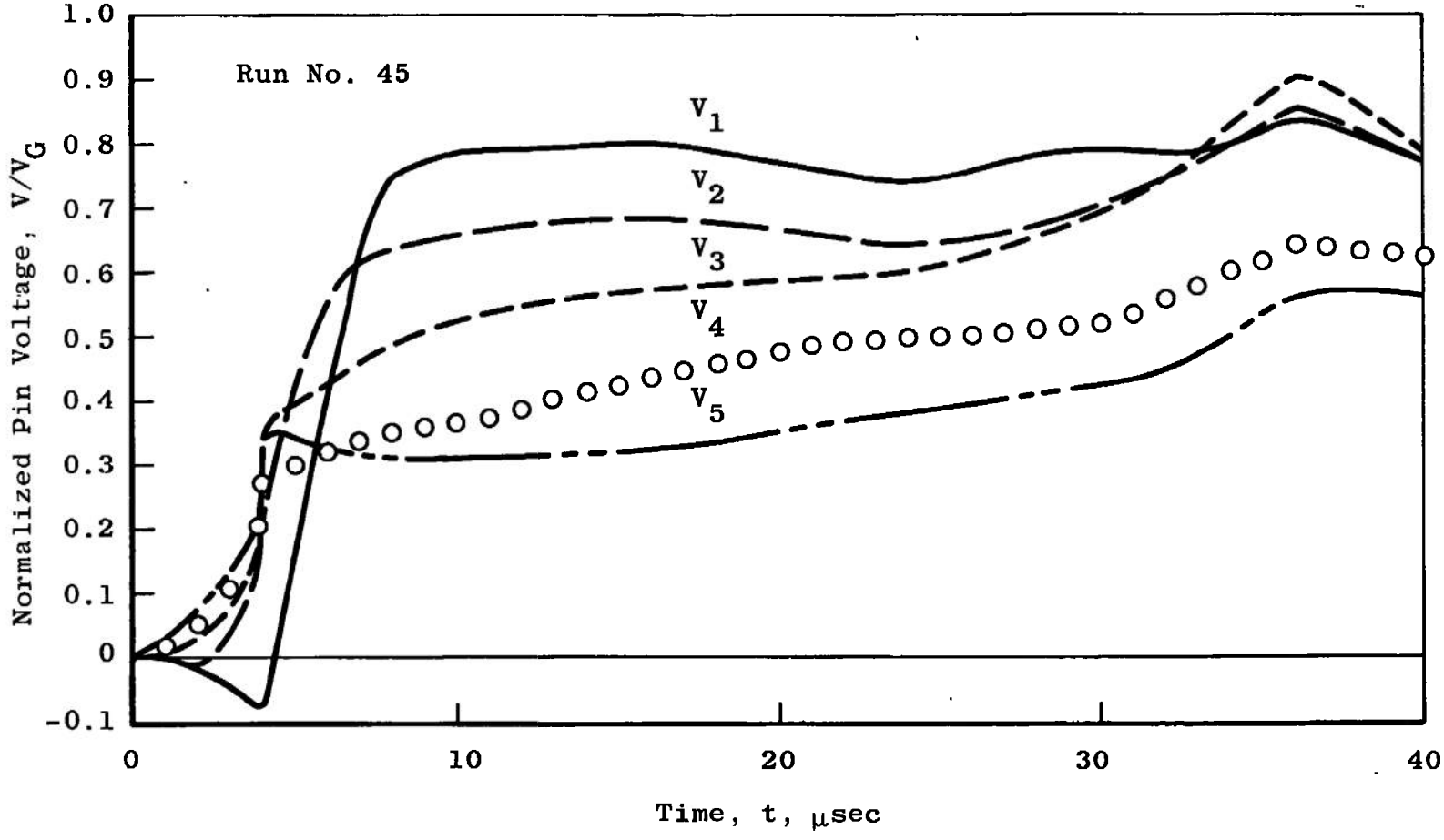


a. Initial Voltage 400 v

Fig. 18 Variation of Normalized Pin Voltage with Time

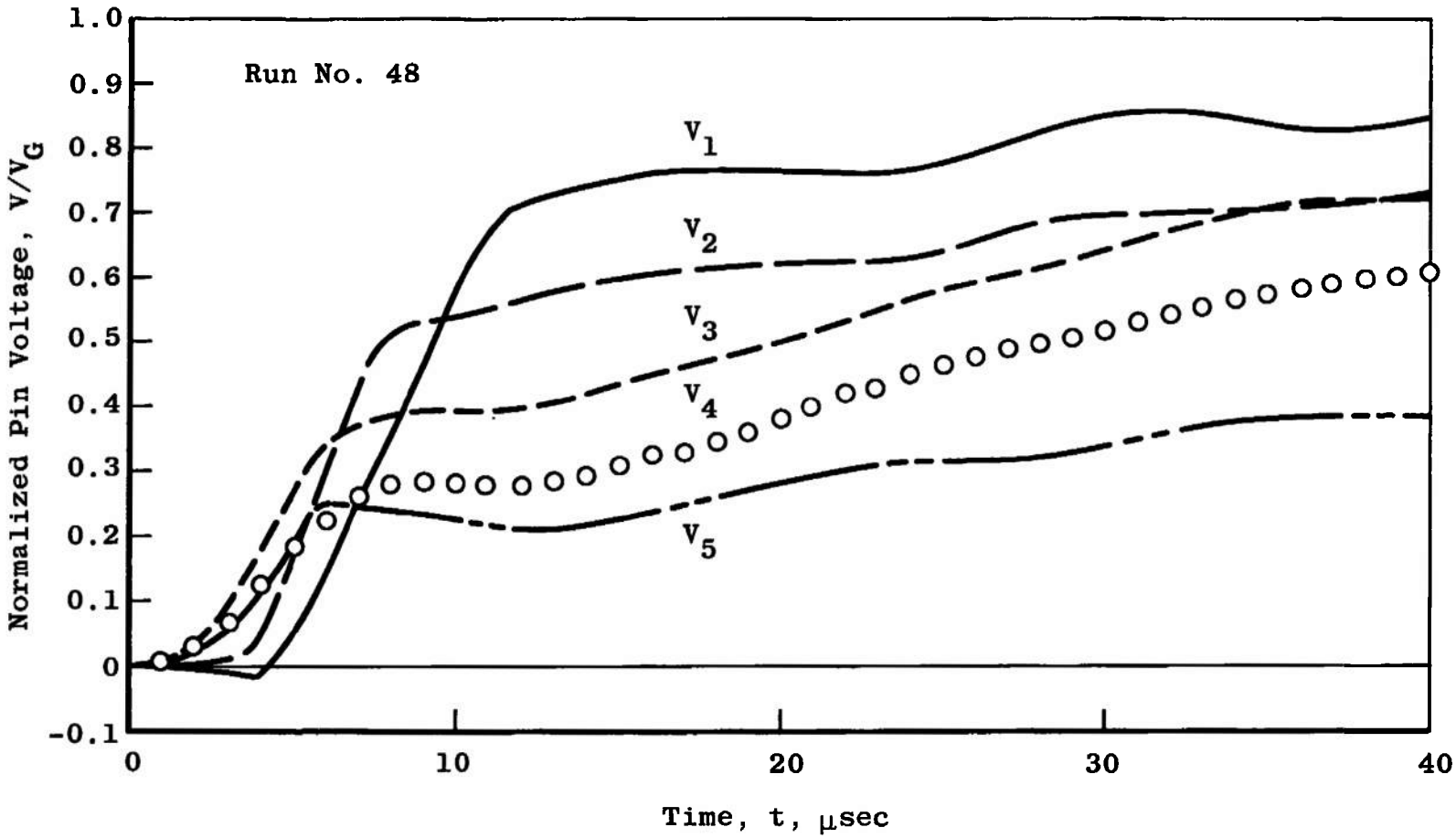


b. Initial Voltage 600 v

Fig. 18 Continued

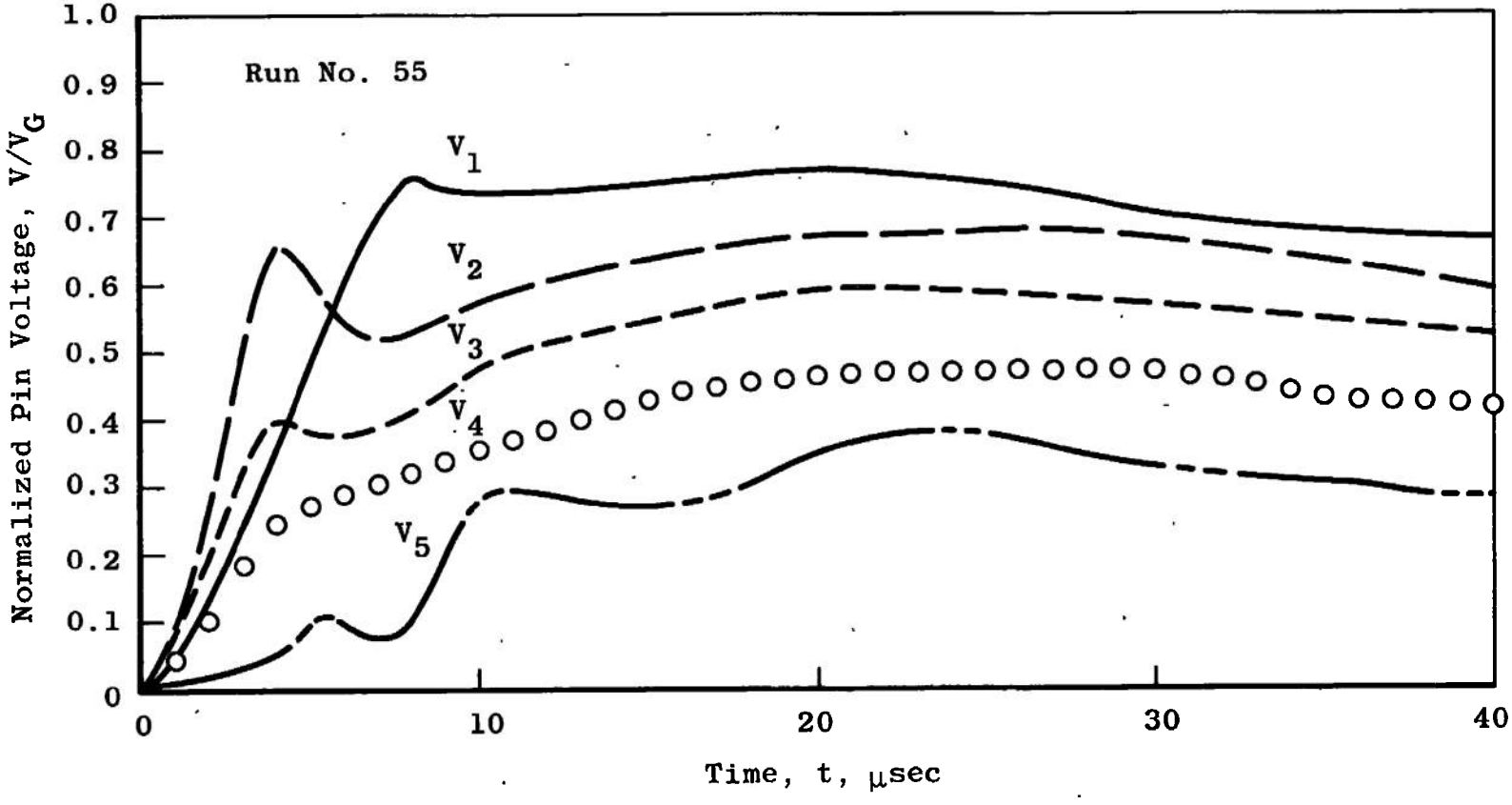


c. Initial Voltage 800 v

Fig. 18 Concluded

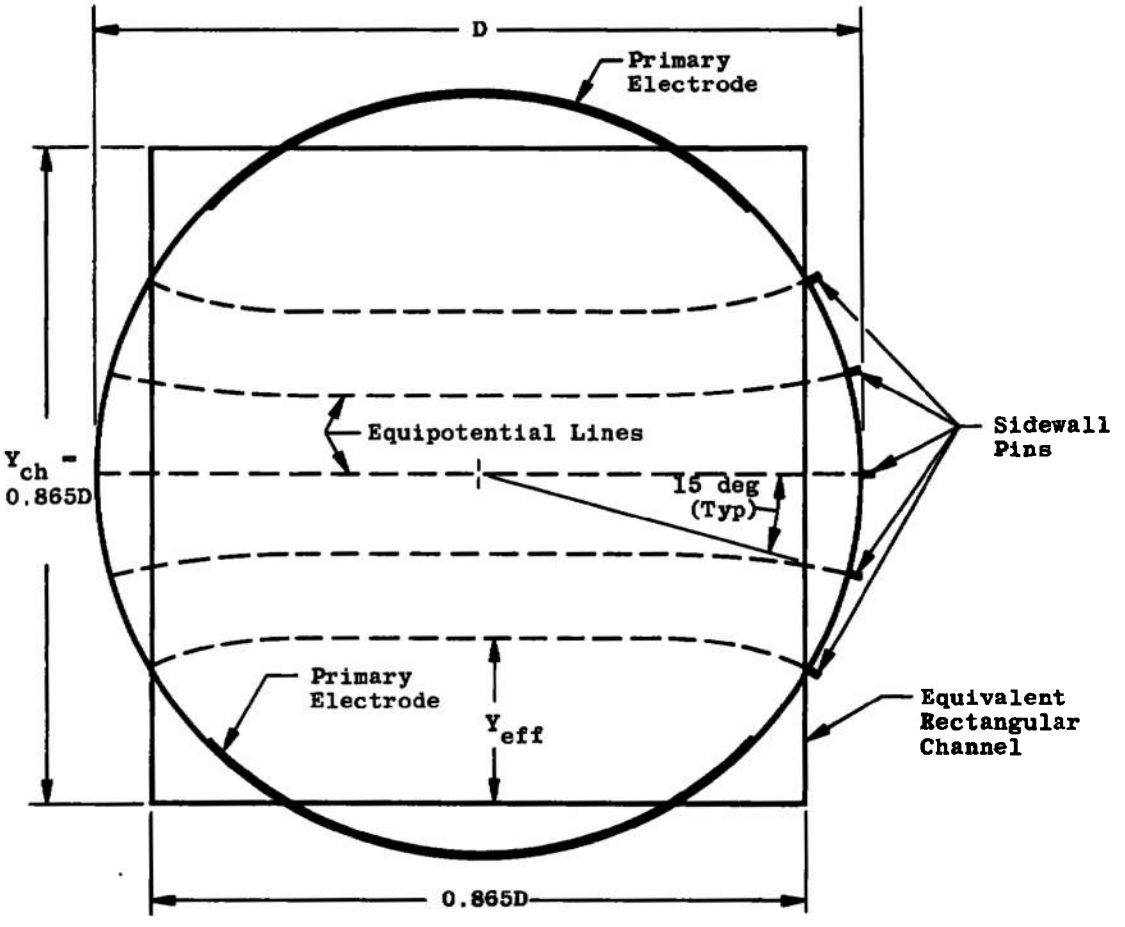


Fig. 19 Equipotential Lines and Equivalent Rectangular Channel

Following assumption b, the potential, V, across the channel can be expressed as the sum of three parts.

$$V_G = \int E \, dy \tag{33}$$

$$\approx E_\infty Y_{CH} + \Delta V_{BL} + \Delta V_{sheath} \tag{34}$$

where

$$\Delta V_{BL} = \Delta V_A + \Delta V_C$$

Here, the subscripts A and C denote anode and cathode boundary layers, respectively.

By using assumption c and the simple Ohm's law, the electric field, $E_\infty$, can be expressed as

$$E = J_\infty/\sigma_\infty$$

$$= I/A_e\sigma_\infty$$

in which $A_e$ is the area of the effective electrodes. Therefore,

$$V_G = \frac{I Y_{CH}}{A_e \sigma_\infty} + \Delta V_{BL} + \Delta V_{sheath} \tag{35}$$

The channel resistance may be expressed in the following form

$$R = \frac{Y_{CH}}{\sigma_e A_e} + \frac{\Delta V_{BL}}{I} + \frac{\Delta V_{sheath}}{I} \tag{36}$$

A major problem in this experiment was the lack of an accurate measurement of the seed mass fraction. Concentrations of seed mass and mass fractions were undoubtedly not consistent from shot to shot. For this reason, the data are displayed graphically with initial electrode voltage, $V_i$, as the grouping parameter. However, it can be noted in Table II that the voltage across the channel at 20 $\mu$sec varied for a fixed applied voltage. This is attributed to variations in conductivity caused by variations in shock strength and seed fractions.

The voltage distribution data are given in Fig. 20. The voltages have been normalized by the voltage across the electrodes, and the data are plotted at the relative pin location in the equivalent rectangular channel (Fig. 19). The results of Fig. 20a for an initial charge voltage of 100 v show a small excess voltage drop in the vicinity of the anode and a significantly larger excess drop in the vicinity of the cathode. Figure 20b, for an initial charge voltage of 200 v, shows a similar trend but the excess voltage drops are proportionally smaller. At the higher initial voltages, the distributions become more linear (Figs. 20c through e). This trend is consistent with the model given by Eq. (35), which has one term proportional to current and two other terms which are relatively constant. As the voltages and currents increase, the constant voltage

drops become proportionally less important. The same trends are noted in the overall conductivity values given in Fig. 21, which were calculated using the total voltage drop and current, with the equivalent rectangular geometry. As the current increases, the apparent conductivity increases.

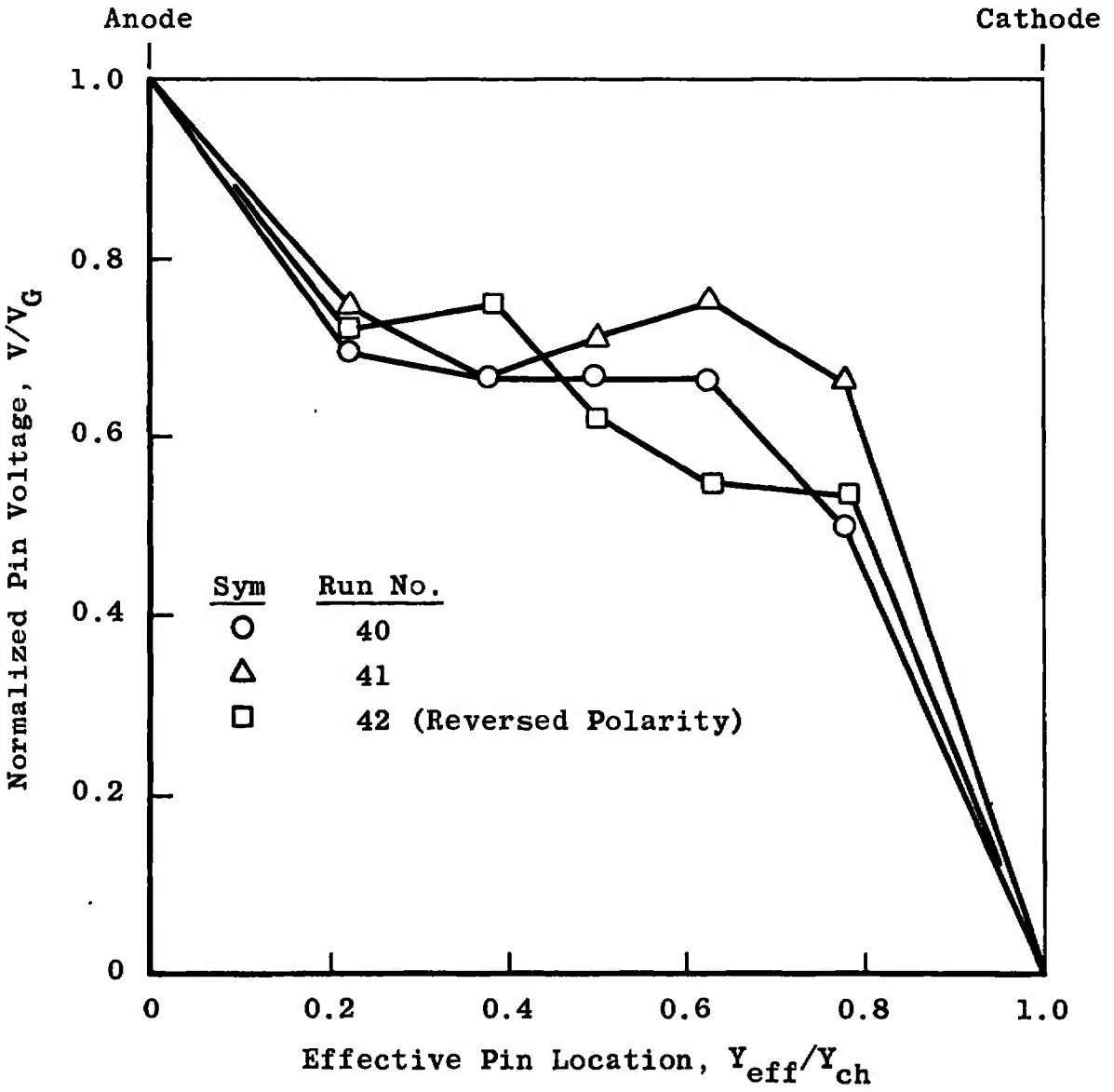


a. Initial Voltage 100 v

Fig. 20 Voltage Distribution Data

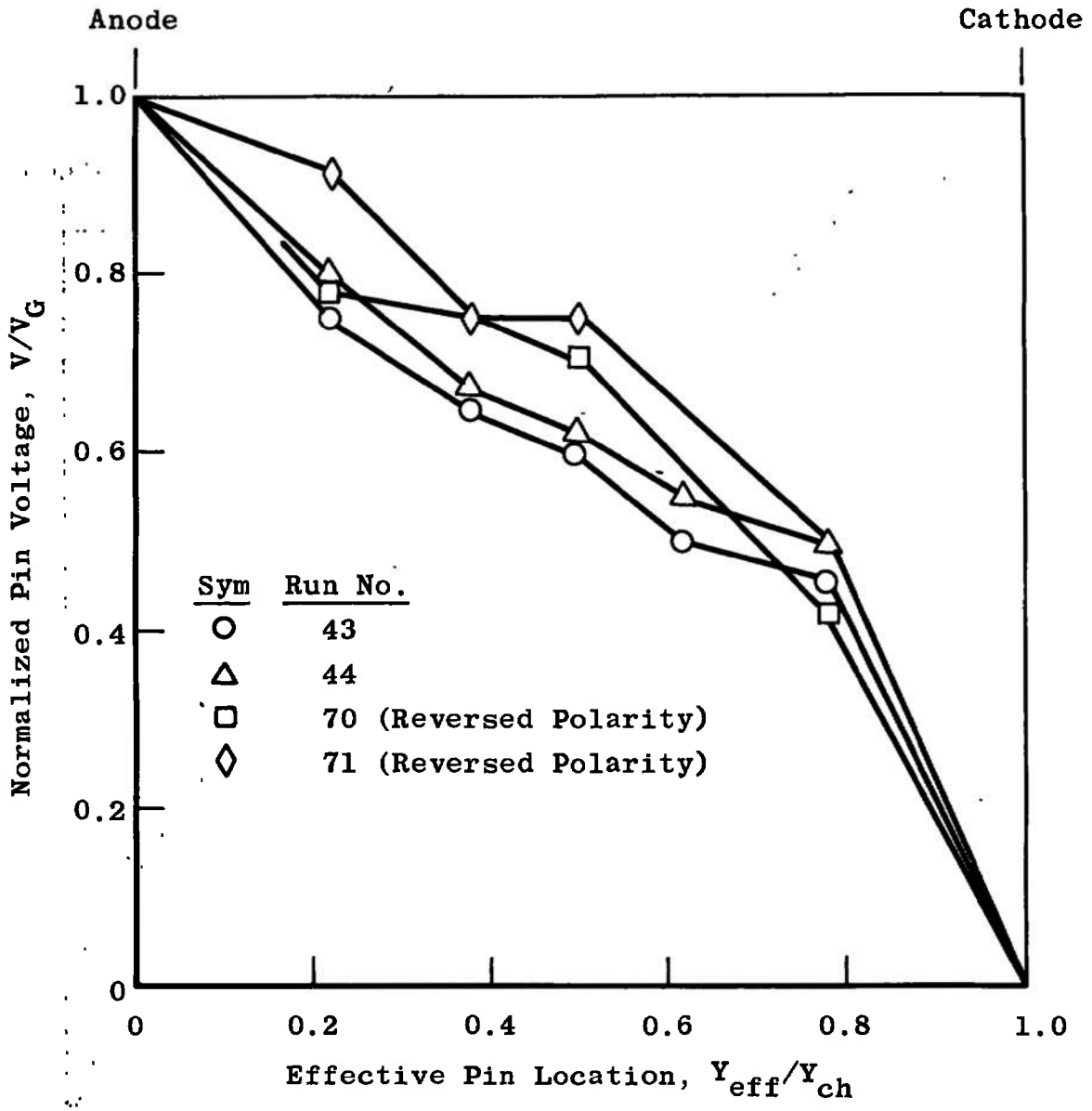


b. Initial Voltage 200 v

Fig. 20 Continued

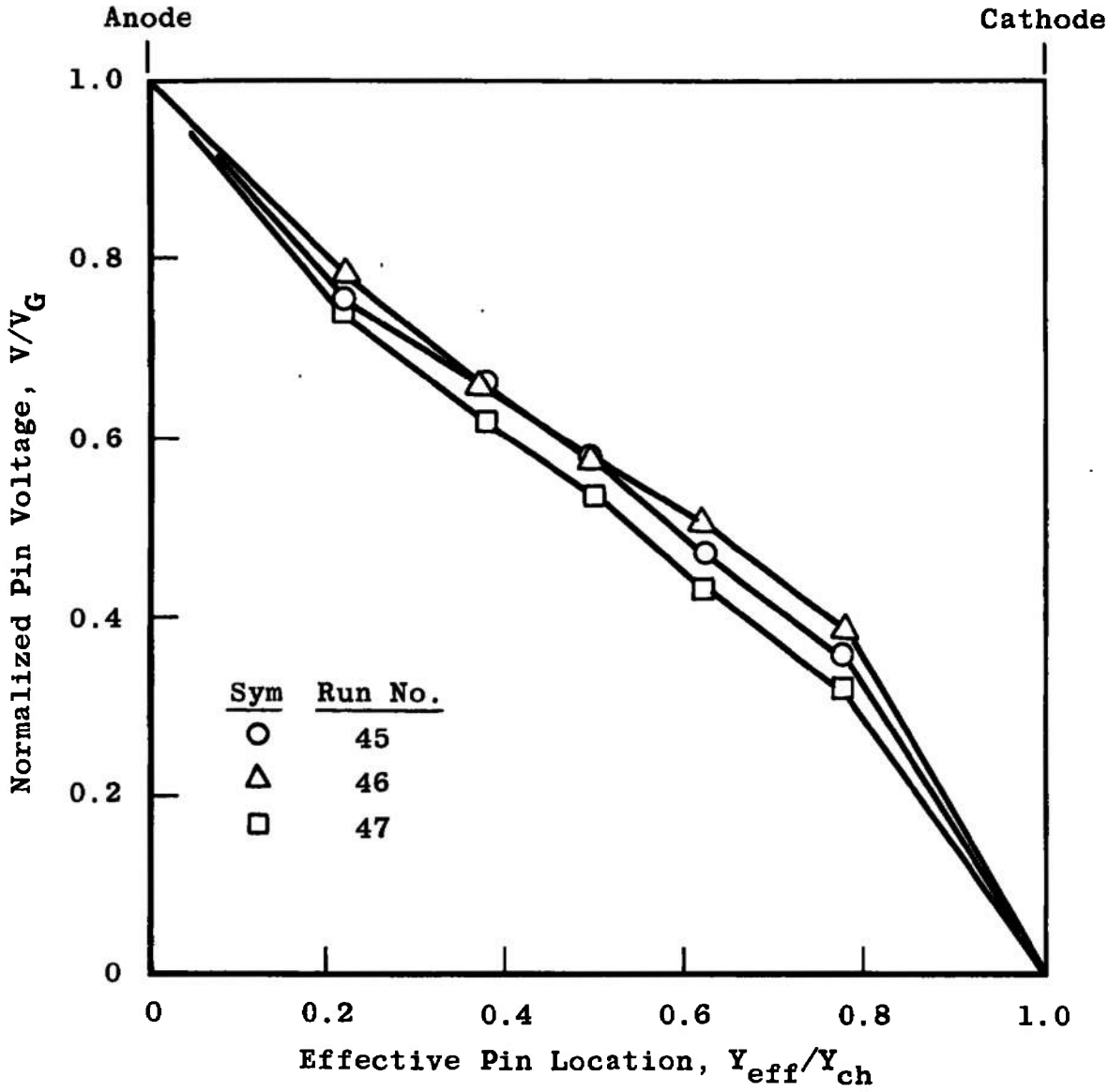


c. Initial Voltage 400 v

Fig. 20 Continued

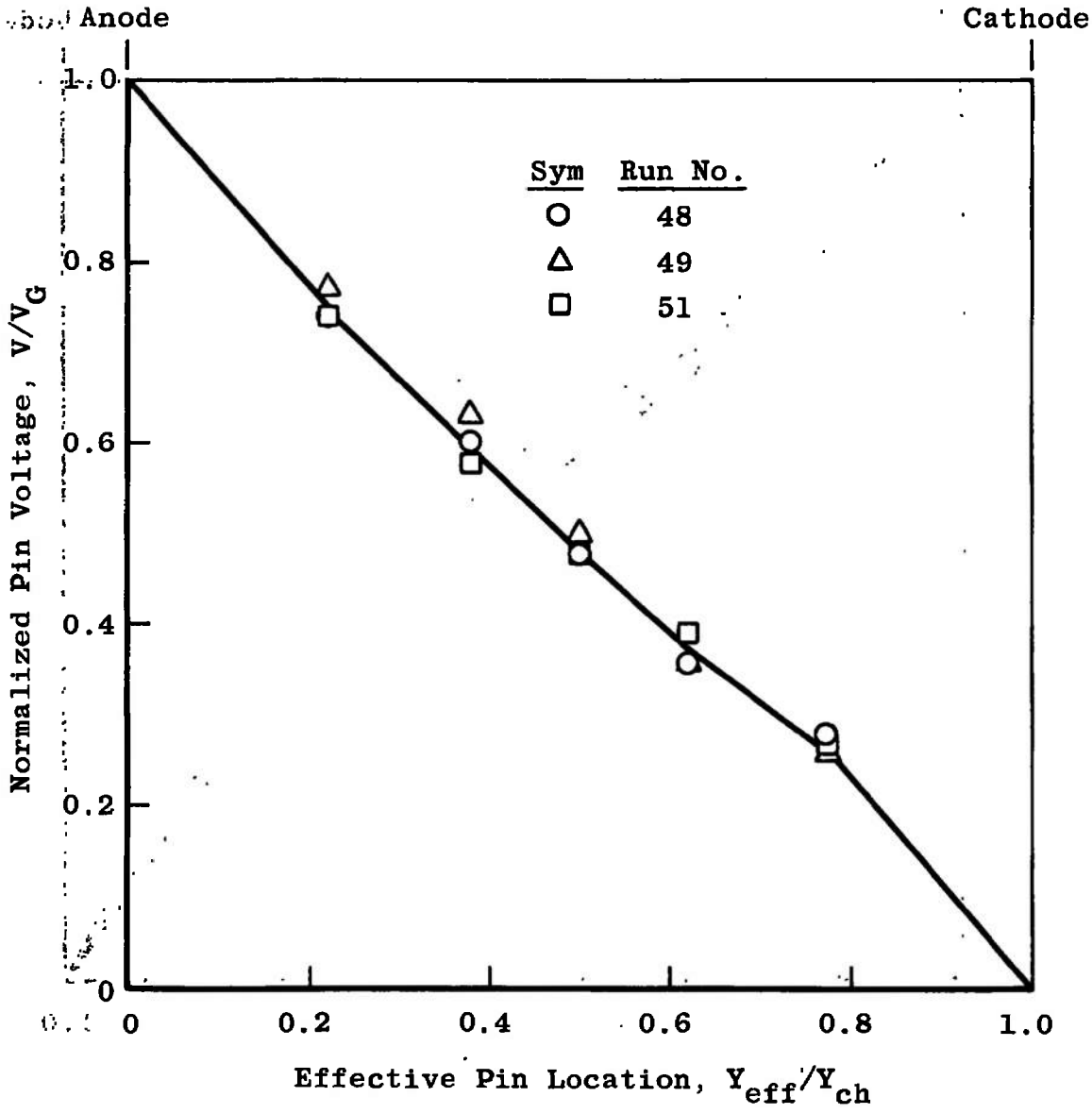


d. Initial Voltage 600 v

Fig. 20 Continued

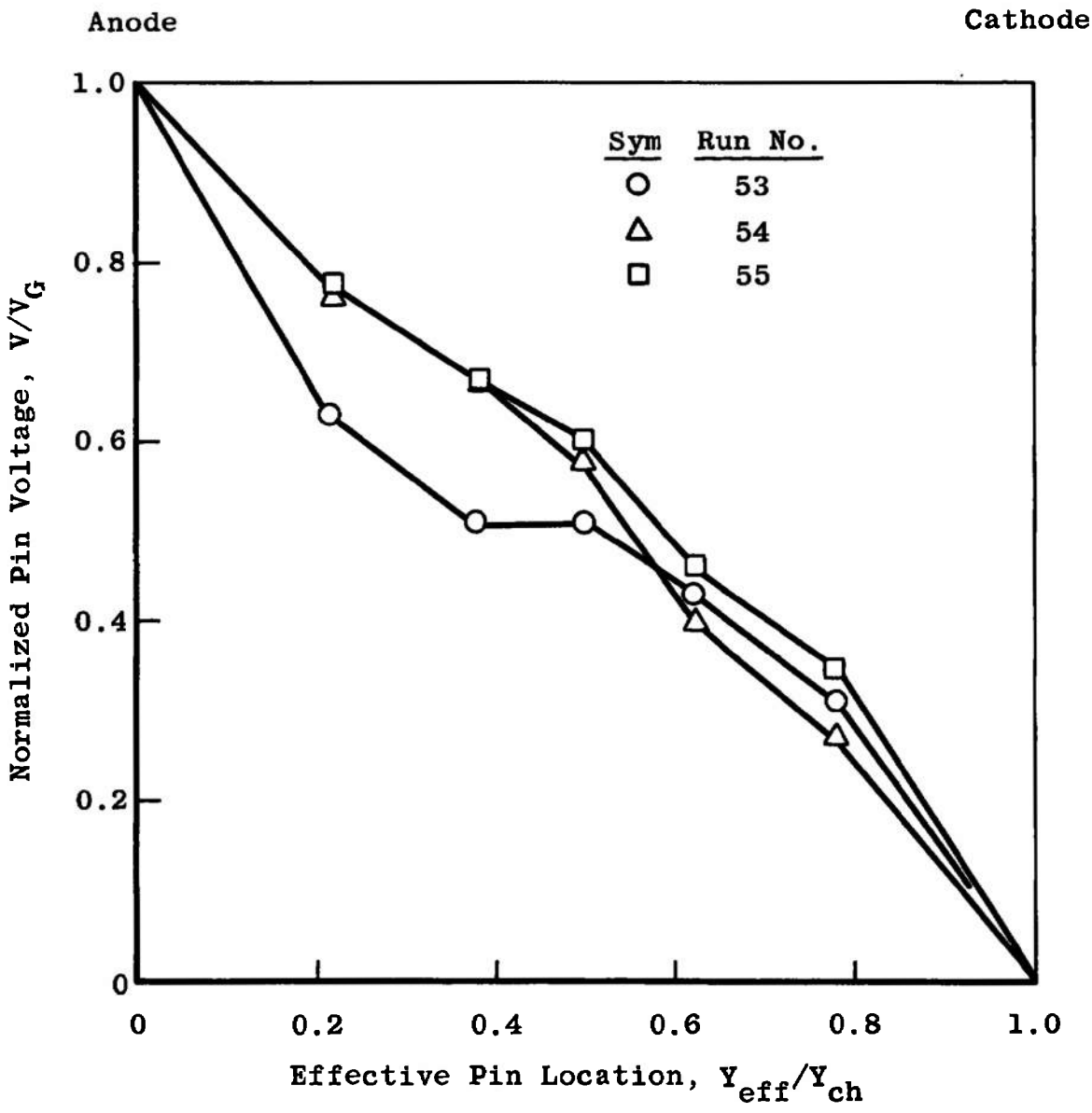


e. Initial Voltage 800 v

Fig. 20 Concluded

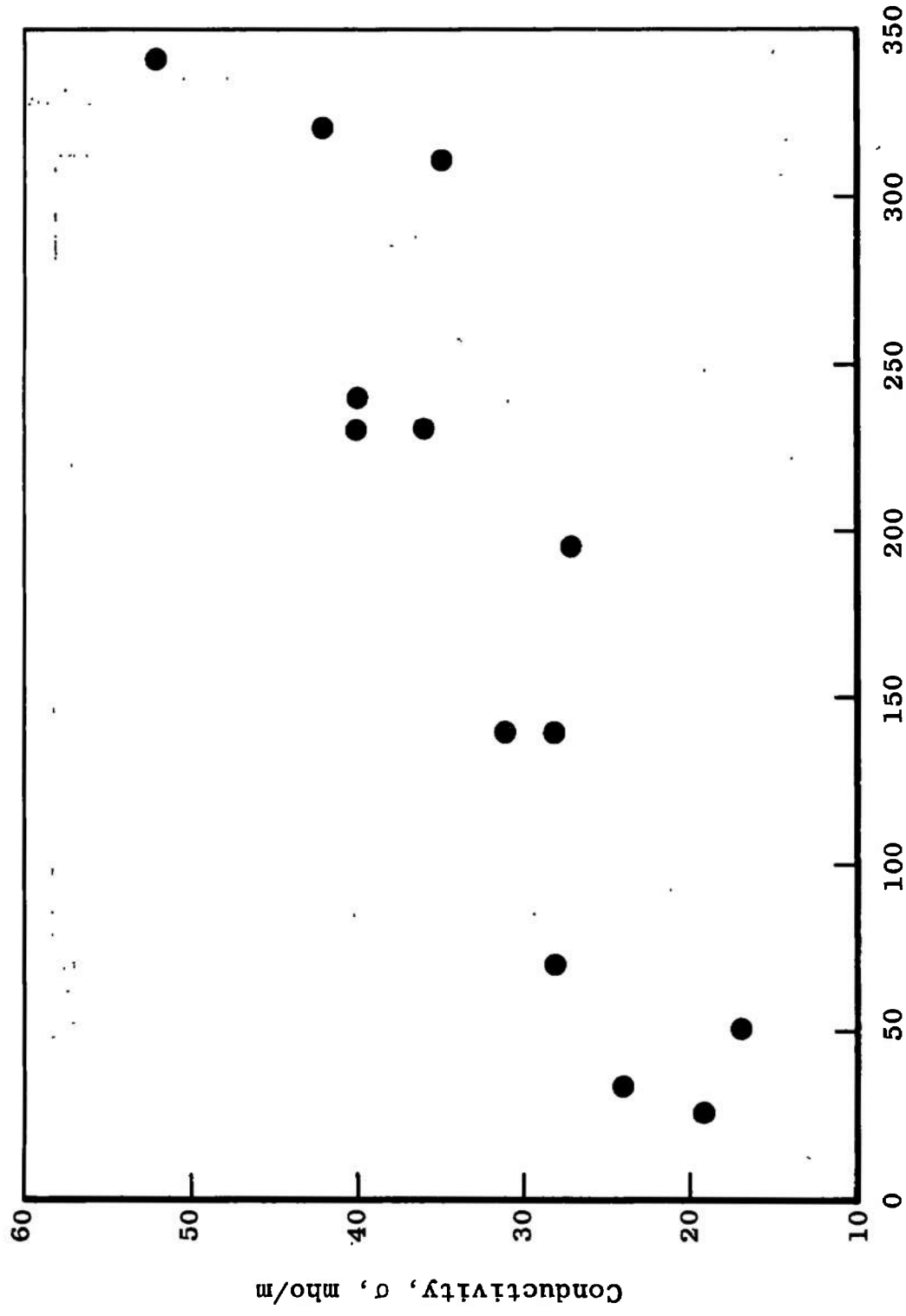


Fig. 21 Overall Conductivity

Despite the high degree of scatter in the data, an attempt was made to determine mean values for the excess voltage drops. First, in order to establish the core conductivity, the voltage difference between pins 1 and 5 was used to determine the conductivity of the gas in a region away from boundary layers. The resulting values are given as the square symbols in Fig. 22. The scatter is fairly large, as might be expected on the basis of the previous results given in Fig. 16. The values range from 20 to 80 mho/m, with most of the data between 35 and 55 mho/m. A mean value of 45 mho/m was chosen. This value is below the anticipated values of 100 to 200 mho/m (Fig. 14). No consistency with shock Mach number was noted. Next, the voltage difference between each electrode and the adjacent pin was plotted versus current. The results are given in Fig. 23. The open circles are the values from the anode to the next pin, and the solid circles are the values for the pin adjacent to the cathode. The voltage differences increase with increasing current, but much of this increase can be attributed to the increased voltage drop in the core. The resulting voltage assuming a conductivity of 45 mho/m for the core drop is shown on the figure.

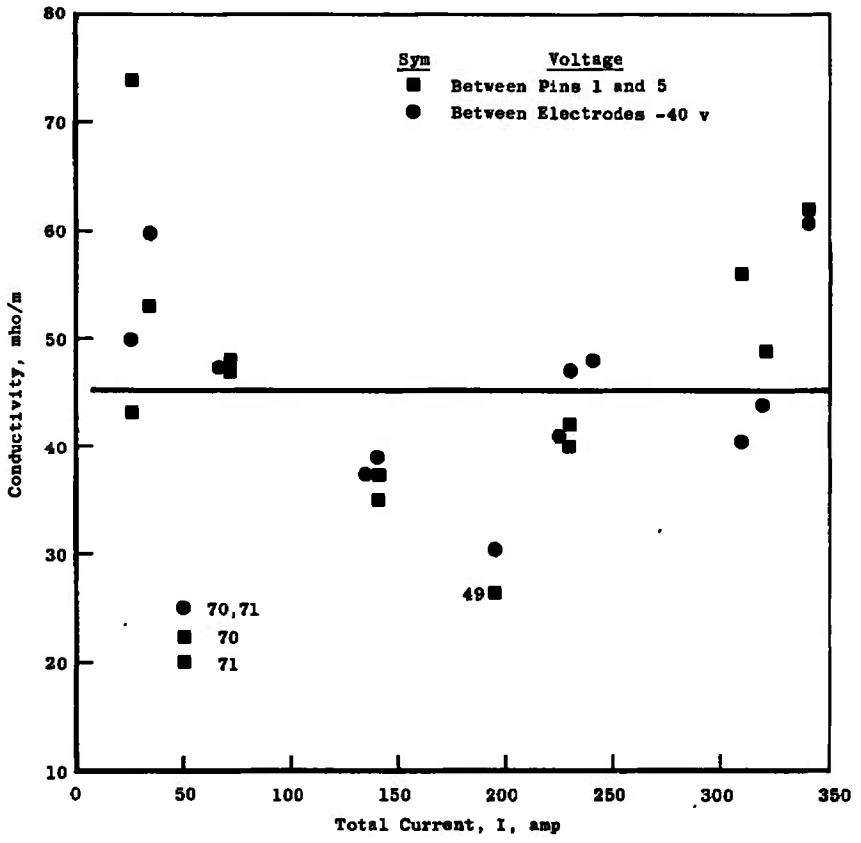


Fig. 22 Core Conductivity

It is difficult to assign very precise numbers to the excess voltage drops on the basis of the data given in Fig. 23. The two other lines are drawn for excess voltage drops of 10 v for the anode and 30 v for the cathode. The data could perhaps be fitted better with larger excess voltage drops and conductivities.

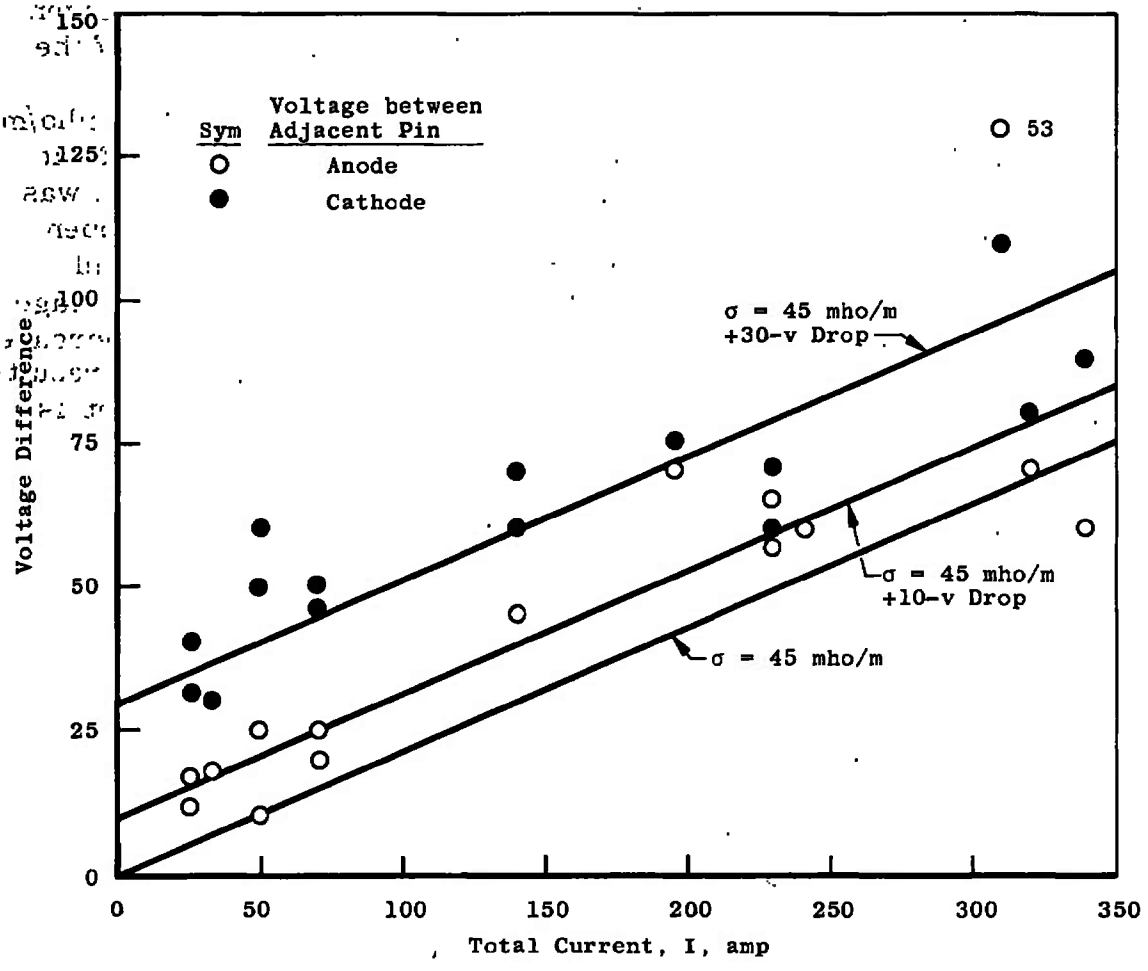


Fig. 23 Voltage Differences at Electrodes

Using a constant overall excess voltage drop of 40 v, the overall core conductivity can be calculated by subtracting this excess voltage drop from the electrode voltage difference. These results are given as the circles in Fig. 22. The results agree reasonably well with those based upon the voltage differences between pins 1 and 5. There are three runs (49, 70, and 71) which are somewhat different.

The mean value of the conductivity in Fig. 22 is about 45 mho/m. This value is less than the expected values of 80 to 150 mho/m. The

values based upon the resistance between pins 1 and 5 are given as crosses in Fig. 12 along with values obtained by the conductivity coil discussed previously. These values are in reasonable agreement with the open circles, but it should be recalled that the values denoted by the open circle were obtained at lower initial pressures. For the initial pressures of 0.2 psia, values of from 70 to 110 mho/m were obtained by the coil. The reason for the discrepancy between the two results has not been found. It is unlikely that it could be attributed to poor seeding. It is possible that for the particular geometry used, a blowing of the discharge downstream could occur with the result that the effective electrode length would be less than the geometric length. This possible explanation has not been explored.

These results clearly indicate that the excess voltage drop at the cathode is greater than that at the anode. Previous studies in argon boundary layers (Refs. 4 through 6) have shown equal excess drops at the anode and cathode. The preliminary results of Ref. 29 for unseeded air also indicate a symmetrical electric field distribution. Others (Refs. 8 and 9) postulate an electric field distribution similar to that found here. In order to verify the asymmetry of the distribution, three runs (42, 70, and 71) were made with the electrode leads reversed and everything else the same. As may be seen by examining the results in Table II, the largest drop remained with the cathode.

The excess voltage drop attributable to the thermal boundary layer is the same for the anode and cathode. From Fig. 15, the theoretical value is from 12 to 20 v for both, or 6 to 10 v for each. The experimentally determined value of 10 v for the anode is in reasonable agreement with this value, but this cannot be taken as verification of the calculations. The additional drop of 20 v at the cathode is not at all unreasonable (Ref. 30) for some cathode sheath phenomena. The total excess voltage drop can therefore be considered as composed of a 20-v cathode sheath drop and the excess voltage drop associated with the thermal boundary layer. However, the data are not precise enough to determine the relative influences of the sheath and the thermal boundary layer.

### 3.5 COMPARISON WITH OTHER RESULTS

There are few experiments with which the present results may be compared. There have been studies in argon (Refs. 4 through 6), but comparisons are not considered worthwhile because of the large differences in the values of $\delta$. Experiments in stagnant air (Ref. 31) are also not considered, because of the differences in the boundary layers.

There are two experiments which can be considered. The first of these was performed by Templemeyer et al. (Ref. 7) in seeded nitrogen and the second by Harris (Ref. 19) in unseeded air.

In order to compare the present experiments with these previous experiments, some common basis must be found. Here the voltage-current relation given by Eq. (35) is used. For all three cases, the channel geometry (equivalent channel for the present tests) is square, so that Eq. (35) becomes

$$V_G = \Delta V + I/\sigma_\infty \ell$$

in which $\Delta V$ is the total sheath and boundary-layer voltage drop, and $\ell$ is the electrode length.

For both of the other experiments, the actual core conductivity and calculated conductivity were in reasonable agreement, so that the value of $\sigma_\infty$ used was a calculated value. This was not so for the present tests, so that the actual value used was that determined from the voltage drop between pins 1 and 5. Note, however, that this is used in conjunction with the geometric length $\ell$, so that the $\sigma_\infty \ell$ product is correctly matched to agree with the resistance of the core.

For all cases, the slope of the curve $V_G$ versus $I/\sigma_\infty \ell$ should be +1. The results are given in Fig. 24. The data for unseeded air are denoted by filled circles. A straight line fit gives a voltage drop at zero current of about 95 v. The seeded nitrogen data are denoted by filled diamonds and give a voltage drop at zero current of about 40 v. The present results for seeded air are denoted by open squares and also give about 35-40 v for the zero current voltage drop.

The seeded nitrogen and seeded air experiments give about the same total drop at the electrodes. The estimated excess voltage drops attributable to the thermal boundary layers are 9 v for nitrogen, and 20 v for air.

The experiments in unseeded air give significantly higher excess voltage drops than the experiments in seeded gases. This is perhaps not too surprising, since the conduction across the thermal boundary layer is somewhat different. In unseeded air, the primary source of electrons is the ionization of NO to $NO^+$. Therefore, NO acts like a seed material. However, in the colder portion of the boundary layer, the amount of NO will be considerably reduced, if equilibrium of the gas composition is maintained. The conductivity will then be significantly reduced. As yet the problem of conduction across an nonionized air boundary layer has not been investigated. Mechanisms that need investigation are (1) the

mechanism used here for seeded air (it is not clear whether elevated concentrations of NO should be included); (2) diffusion of electrons into the boundary layer from the core flow, and (3) arcs.

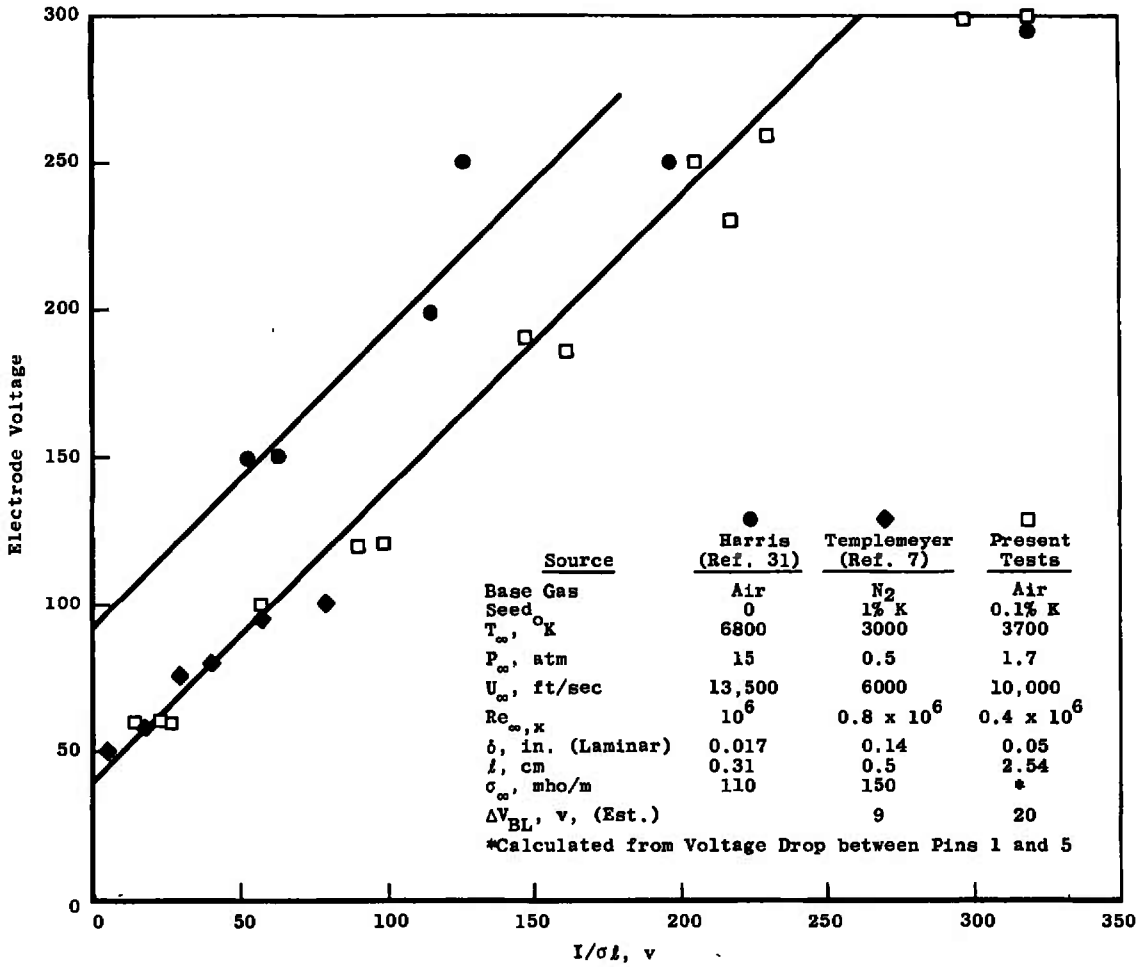


**Fig. 24 Comparison of Voltage Distribution Data**

The data for seeded nitrogen and seeded air indicate a flattening out of the voltage-current curve. This is probably attributable to an elevated electron temperature in the free stream (Ref. 7).

### 3.6 SUMMARY OF EXPERIMENTAL RESULTS

These results have shown that the voltage drop at the cathode is larger than that at the anode, which indicates the occurrence of some sheath phenomena. The voltage drop associated with the sheath is larger than the predicted excess boundary-layer voltage drop. This

fact, coupled with the scatter of the experiments, precludes making firm conclusions about the excess boundary-layer voltage drop. The results do show that adding a value for the sheath drop of 20 v to the excess boundary-layer voltage drop gives a value in reasonable agreement with the experimental results.

Two aspects which have not as yet been satisfactorily explained are the short run time, as shown in Fig. 17, and the values for conductivity lower than estimated.

## SECTION IV
## CONCLUDING REMARKS

The study reported on herein was undertaken in order to provide information for selecting energy supplies for an MHD accelerator operating with seeded air. The results show that for a laminar boundary layer at a static pressure of 2 atm, the voltage of the energy supply should be increased by approximately 30 to 50 v, to allow for the sheath drop and the excess boundary-layer voltage drop associated with the thermal boundary layer on the electrodes. As the pressure level inside the accelerator is increased, the excess boundary-layer voltage drop also increases, but at some pressure level, the boundary layer becomes turbulent, and for a turbulent boundary layer, the excess boundary-layer voltage drop is expected to be small.

## REFERENCES

1. Lam, S. H. "A General Theory for the Flow of Weakly Ionized Gas." AIAA Journal, Vol. 2, No. 3, March 1964, pp. 256-259.

2. Lin, J. T. C. "On Shock Tube Sidewall Langmuir Probes." Princeton University G. D. L. Report 764, January 1964.

3. Argyropoulos, G. S., Demetriades, S. T., and Kendid, A. P. "Current Distribution for Crossed-Field Accelerators (Part 1, Effects of Thermal Diffusion and Boundary Layers)." Vol. I. AEDC-TR-67-135 (AD818907), July 1967.

4. Denison, Richard M. and Ziemer, R. W. "Invesitgation of the Phenomena in Crossed-Field Plasma Accelerators." AIAA Paper No. 63-378, Fifth Biennial Gas Dynamics Symposium, August 1963.

5. Hoffman, M. A. and Oates, G. C. "Electrode Current Distributions in MGD Channels." NASA-CR-69996, January 1966.

6. Goldstein, R., Richmond, J. K., and Oates, G. C. "Electrical Conductivity Measurements in a Faraday Accelerator." AIAA Paper No. 66-75, January 1966.

7. Tempelmeyer, K. E., Whoric, J. M., Rittenhouse, L. E., and McKee, M. L. "Some Characteristics of an Electrical Discharge Transverse to a Supersonic Seeded Nitrogen Plasma Stream with Cold-Copper Electrodes." AEDC-TR-65-52 (AD459312), March 1965.

8. Pain, H. T. and Smy, P. R. "Experiments on Power Generation from a Moving Plasma." Journal of Fluid Mechanics, Vol. 10, 1961, pp. 51-59.

9. George, D. W. and Messerle, H. K. "Electrode Conduction Processes in Plasmas." Journal of Fluid Mechanics, Vol. 13, 1962, pp. 465-477.

10. Brogan, T. R. "The Conduction of Electrical Current to Cold Electrodes in Shock Tubes." Cornell University Thesis, 1956.

11. Hurwitz, H., Kilb, R. W., and Sutton, G. E. "Influence of Tensor Conductivity on Current Distribution in a MHD Generator." Journal of Applied Physics, Vol. 32, 1961, pp. 205-216.

12. Kerrebrock, J. L. "Conduction in Gases with Elevated Electron Temperature." Proceedings of the Second Symposium on the Engineering Aspects of Magnetohydrodynamics, New York, New York; Columbia University Press, 1962.

13. Weber, R. E. and Tempelmeyer, K. E. "Calculation of the D-C Electrical Conductivity of Equilibrium Nitrogen and Argon Plasma with and without Alkali Metal Seed." AEDC-TDR-64-119 (AD602858), July 1964.

14. Spitzer, Lyman, Jr. Physics of Fully Ionized Gases. Interscience Publishers, Division of John Wiley and Sons, New York, 1962 (Second Edition, No. 3).

15. Ginzburg, V. L. and Gureirck, A. V. "Nonlinear Phenomena in Plasma in a Variable Electromagnetic Field." (English Translation: Soviet Phys. Usp. Vol. 3, 1960, pp. 115-146 and 175-194).

16. Whitehead, G. L. "Computer Programs for the Performance Calculation of MHD Channel Flow." University of Tennessee Thesis for the degree of Master of Science, 1967.

17. Schkarofsky, I. P., Bochynski, M. P., and Johnson, T. W. R. C. A. Research Report 7-8015, 1960.

18. Crocco, L. "Transmission of Heat from a Flat Plate to a Fluid Flowing at a High Velocity." (translation) NACA TM-690, 1932.

19. Harris, C. J. Private Communication.

20. Norfleet, Glenn D., Lacey, John J., Jr., and Whitfield, Jack D. "Results of an Experimental Investigation of the Performance of an Expansion Tube." AEDC-TR-66-10 (AD628628), February 1966.

21. Smithson, H. K. "Experiments on Shock Tube Seeding." AEDC-TR-67-205 (AD822083), October 1967.

22. Lin, S. C., Resler, E. L., and Kantrowitz, A. "Electrical Conductivity of Highly Ionized Argon Produced by Shock Waves." Journal of Applied Physics, Vol. 26, January 1955.

23. Glass, I. I. and Hall, J. G. "Handbook of Supersonic Aerodynamics." NAVORD Report 1488, Vol. 6, December 1959.

24. White, Donald R. "Influence of Diaphragm Opening Time on Shock Tube Flow." Journal of Fluid Mechanics, Vol. 4, Part 6, November 1958.

25. Lewis, C. H. and Burgess, E. G., III. "Charts of Normal Shock Wave Properties in Imperfect Air." AEDC-TDR-64-43 (AD433958), March 1964.

26. Hartunian, R. A., Russo, A. L., and Marrone, P. V. "Boundary Layer Transition and Heat Transfer in Shock Tubes." Journal of the Aerospace Sciences, Vol. 27, August 1960, pp. 587-594.

27. Mirels, H. "Test Time in Low Pressure Shock Tubes." Physics of Fluids, Vol. 6, 1963, pp. 1201-1214.

28. Fishman, Frank. "Steady Magnetohydrodynamic Flow through a Channel of Circular Section." AVCO Research Report No. 97, AFBMD TR-61-13, December 1960.

29. General Electric Company Space Sciences Laboratory. "Feasibility Study of a High Density Shock Tunnel Augmented by a Magnetohydrodynamic Accelerator." AEDC-TR-65-225 (AD472465), October 1965.

30. Zauderer, Bert. "Electrical Characteristics of Linear Hall and Faraday Generators at Small Hall Parameters." AIAA Journal, Vol. 5, No. 3, March 1967.

31. Selamoglu, S. "Experiments on Joule Heating of Shock Ionized Air." Brown University Technical Report WT-45, March 1966.

# APPENDIX
# TABLES

## TABLE I
## EXCESS VOLTAGE DROP FOR TURBULENT BOUNDARY LAYERS

| P, atm | J, amp/cm$^2$ | Nitrogen | | Air | |
|---|---|---|---|---|---|
| | | $\Delta V_{BL}$ (Vcm) $T_{\infty j}$ = 3500 deg | $\Delta V_{BL}$ (Vcm) $T_\infty$ = 4000°K | $\Delta V_{BL}$ (Vcm) $T_\infty$ = 3500 deg | $\Delta V_{BL}$ (V/cm) $T_\infty$ = 4000°K |
| 0.1 | 0.1 | 0.00 | 0.00 | 0.00 | 0.00 |
| | 0.3 | 0.00 | 0.01 | 0.01 | 0.01 |
| | 0.7 | 0.01 | 0.01 | 0.03 | 0.02 |
| | 1.0 | 0.02 | 0.01 | 0.05 | 0.03 |
| | 3.0 | 0.03 | 0.03 | 0.12 | 0.09 |
| | 7.0 | 0.03 | 0.03 | 0.20 | 0.15 |
| | 10.0 | 0.03 | 0.02 | 0.21 | 0.17 |
| | 30.0 | --- | --- | 0.06 | 0.11 |
| 1.0 | 0.1 | 0.01 | 0.01 | 0.01 | 0.01 |
| | 0.3 | 0.03 | 0.02 | 0.03 | 0.02 |
| | 0.7 | 0.06 | 0.04 | 0.07 | 0.04 |
| | 1.0 | 0.09 | 0.06 | 0.09 | 0.06 |
| | 3.0 | 0.18 | 0.16 | 0.28 | 0.18 |
| | 7.0 | 0.31 | 0.32 | 0.63 | 0.41 |
| | 10.0 | 0.36 | 0.42 | 0.86 | 0.59 |
| | 30.0 | 0.44 | 0.78 | 1.78 | 1.53 |
| | 70.0 | 0.39 | 0.80 | 2.17 | --- |
| 10.0 | 0.1 | 0.04 | 0.02 | 0.03 | 0.01 |
| | 0.3 | 0.10 | 0.07 | 0.08 | 0.04 |
| | 0.7 | 0.22 | 0.16 | 0.19 | 0.10 |
| | 1.0 | 0.29 | 0.21 | 0.27 | 0.15 |
| | 3.0 | 0.73 | 0.59 | 0.81 | 0.44 |
| | 7.0 | 1.45 | 1.27 | 1.88 | 1.02 |
| | 10.0 | 1.88 | 1.74 | 2.66 | 1.45 |
| | 30.0 | 3.63 | 4.40 | 7.34 | 4.31 |
| | 70.0 | 4.66 | 8.10 | 13.64 | --- |
| 100.0 | 0.1 | 0.14 | 0.08 | 0.09 | 0.05 |
| | 0.3 | 0.39 | 0.25 | 0.26 | 0.15 |
| | 0.7 | 0.81 | 0.56 | 0.61 | 0.35 |
| | 1.0 | 1.11 | 0.77 | 0.87 | 0.50 |
| | 3.0 | 2.84 | 2.11 | 2.61 | 1.49 |
| | 7.0 | 5.82 | 4.56 | 6.09 | 3.49 |
| | 10.0 | 17.82 | 6.30 | 8.69 | --- |
| | 30.0 | 18.50 | 16.84 | 25.62 | 14.91 |
| | 70.0 | 32.20 | 34.96 | 55.93 | --- |

## TABLE II
## RESULTS OF VOLTAGE DISTRIBUTION TESTS

| Run No. | Initial Press, $P_1$, mm Hg | $M_s$ | Initial Voltage, $V_1$ | Electrode Voltage, $V_G$ | Pin Voltages | | | | | Current, I, amp | Overall -Resistance, R, Ω | Apparent Conductivity, $\sigma_a$, Ω/m | Mean Current Density, amp/cm$^2$ |
|---|---|---|---|---|---|---|---|---|---|---|---|---|---|
| | | | | | $V_1$ | $V_2$ | $V_3$ | $V_4$ | $V_5$ | | | | |
| 40 | 11 | . | 100 | 60 | 42 | 40 | 40 | 40 | 30 | 32 | 1.7 | 24 | 3.6 |
| 41 | 11 | 9.9 | 100 | 60 | 48 | 40 | 43 | 45 | 40 | 26 | 2.1 | 19 | 3.0 |
| *42 | 11 | 10.0 | 100 | 60 | 32 | 34 | 37 | 46 | 44 | 26 | 2.1 | 19 | 3.0 |
| 43 | 12 | 9.9 | 200 | 100 | 75 | 65 | 60 | 50 | 46 | 70 | 1.4 | 28 | 8.0 |
| 44 | 11.5 | 10.2 | 200 | 100 | 80 | 67 | 62 | 55 | 50 | 70 | 1.4 | 28 | 8.0 |
| *70 | | 9.2 | 200 | 120 | 50 | | 85 | 90 | 95 | 50 | 2.4 | 17 | 5.7 |
| *71 | | 9.8 | 200 | 120 | 60 | | 90 | 90 | 110 | 50 | 2.4 | 17 | 5.7 |
| 45 | 11 | 9.8 | 400 | 190 | 145 | 125 | 110 | 90 | 70 | 140 | 1.4 | 28 | 16.0 |
| 46 | 11 | 9.7 | 400 | 160 | 125 | 105 | 95 | 80 | 60 | | | | |
| 47 | 11 | | 400 | 185 | 140 | 115 | 100 | 80 | 60 | 140 | 1.3 | 31 | 16.0 |
| 48 | 11 | 10.1 | 600 | 250 | 185 | 150 | 120 | 90 | 70 | 230 | 1.1 | 36 | 26.0 |
| 49 | 11.5 | 9.5 | 600 | 300 | 230 | 190 | 150 | 105 | 80 | 195 | 1.5 | 27 | 22.0 |
| 50 | 11 | | 600 | 240 | 180 | 155 | 120 | | | 240 | 1.0 | 40 | 27.0 |
| 51 | 11 | 9.7 | 600 | 230 | 170 | 135 | 110 | 90 | 60 | 230 | 1.0 | 40 | 26.0 |
| 53 | 11 | 9.7 | 800 | 350 | 220 | 180 | 180 | 150 | 110 | 310 | 1.1 | 36 | 35.0 |
| 54 | 11.5 | 9.5 | 800 | 300 | 230 | 200 | 175 | 120 | 80 | 320 | 0.94 | 42 | 36.0 |
| 55 | 11 | 9.5 | 800 | 260 | 200 | 175 | 155 | 120 | 90 | 340 | 0.77 | 52 | 39.0 |

*Reversed polarity

Traces read at 20 μsec after initiation of discharge.

UNCLASSIFIED

Security Classification

**DOCUMENT CONTROL DATA - R & D**

*(Security classification of title, body of abstract and indexing annotation must be entered when the overall report is classified)*

| 1. ORIGINATING ACTIVITY (Corporate author) | 2a. REPORT SECURITY CLASSIFICATION |
|---|---|
| Arnold Engineering Development Center<br>ARO, Inc., Operating Contractor<br>Arnold Air Force Station, Tennessee | UNCLASSIFIED |
| | 2b. GROUP<br>N/A |

3. REPORT TITLE

STUDIES OF ELECTRICAL CHARACTERISTICS OF GASDYNAMIC BOUNDARY LAYERS IN SEEDED DIATOMIC GASES

4. DESCRIPTIVE NOTES (Type of report and inclusive dates)

July 1966 to January 1968 - Final Report

5. AUTHOR(S) (First name, middle initial, last name)

Captain E. E. Goins, USAF and Wendell Norman, ARO, Inc.

| 6. REPORT DATE | 7a. TOTAL NO. OF PAGES | 7b. NO. OF REFS |
|---|---|---|
| June 1968 | 69 | 31 |

| 8a. CONTRACT OR GRANT NO. | 9a. ORIGINATOR'S REPORT NUMBER(S) |
|---|---|
| AF 40(600)-1200<br>b. PROJECT NO. 7778<br>c. Program Element 6241003F<br>d. Task 777807 | AEDC-TR-68-111 |
| | 9b. OTHER REPORT NO(S) (Any other numbers that may be assigned this report)<br>N/A |

10. DISTRIBUTION STATEMENT

This document has been approved for public release and sale; its distribution is unlimited.

| 11. SUPPLEMENTARY NOTES | 12. SPONSORING MILITARY ACTIVITY |
|---|---|
| Available in DDC | AEDC (AETS),<br>Arnold Air Force Station,<br>Tennessee 37389 |

13 ABSTRACT

Calculations are presented of the excess boundary-layer voltage drop attributable to the conduction of current through a thermal boundary layer on the electrodes of an MHD accelerator operating with seeded air or nitrogen, using the two-temperature model of Kerrebrock. For a laminar boundary layer, the excess boundary-layer voltage drop is found to be a linear function of pressure, relatively insensitive to free-stream temperature and seed fraction, and larger for air than for nitrogen. Experiments conducted in a shock tube showed an asymmetry in the voltage distribution for seeded air, with the cathode drop approximately 30 v and the anode drop approximately 10 v.

DD FORM 1 NOV 65 1473

UNCLASSIFIED

Security Classification

| 14. KEY WORDS | LINK A | | LINK B | | LINK C | |
|---|---|---|---|---|---|---|
| | ROLE | WT | ROLE | WT | ROLE | WT |
| voltage drop | | | | | | |
| gasdynamic boundary layers | | | | | | |
| diatomic gases | | | | | | |
| MHD accelerators | | | | | | |
| nitrogen | | | | | | |
| pressure | | | | | | |
| seed fraction | | | | | | |
| temperature | | | | | | |